UNIVERSITAT POLITÈCNICA DE CATALUNYA
BARCELONATECH
Escola Tècnica Superior d'Enginyeria
Industrial de Barcelona

MSc in Industrial Engineering

Final Master Thesis

Control of a Four In-Wheel Motor Drive Electric Vehicle

Supervisors:
Dr. Arnau Dòria-Cerezo
Dr. Josep M. Olm

Author:
Matteo Kevin Ghezzi

September 2017

Abstract

The thesis deals with the direct yaw moment control of a four in-wheel motor independent drive electric vehicle. The advantages of this kind of vehicle are exploited by designing an optimal torque vectoring controller. The torque distribution computation coincides with the resolution of an optimization problem, which is carried out with the use of gradient method. Three different cost functions are taken into account to formulate the optimization problem, while the restrictions are always the same, since they come from physical limitations of the motors and imposed conditions to avoid tire slipping. Two type of controllers are implemented for the direct yaw moment control: a combined PID and sliding mode control, and a model reference adaptive control. The system is simulated in MATLAB/Simulink software, reproducing some common test scenarios like J-turn, single and double lane change. Simulations show that satisfying result are obtained in terms of yaw rate reference tracking and torque distribution curves. Finally, results obtained with the two controllers and the three cost function are compared and commented critically, highlighting points of strength and weaknesses of each solution.

Contents

1 Introduction **1**

2 State of the art **5**
2.1 The 4MIDEV 5
2.2 Torque vectoring control 7

3 Model **9**
3.1 Vehicle dynamics model 9
3.1.1 Longitudinal dynamics 10
3.1.2 Lateral dynamics 11
3.1.3 Tire model: the Pacejka's Magic Formula 14
3.1.4 State-space model 16
3.2 Electric motors 19
3.3 Introduction to control objectives 20
3.3.1 Yaw moment controller 21
3.3.2 Torque vectoring 21

4 Torque vectoring **23**
4.1 Restrictions 23
4.2 Cost functions 26
4.2.1 Longitudinal slip power loss 26
4.2.2 Total tire force coefficient 27
4.2.3 Longitudinal slip standard deviation 28
4.3 Gradient method 29
4.4 Torque allocation via gradient method 30

5 Control **33**
5.1 Control structure 33
5.2 High-level controller 34
5.3 Combined PID and sliding-mode control 35
5.4 Model reference adaptive control 37
5.4.1 Parameter estimation 37
5.4.2 Adaptive algorithm 40

6 Simulations and analysis of the results **43**
6.1 Input signals 44
6.2 Validation of the torque allocation via gradient method 47
6.2.1 Longitudinal slip power loss 47
6.2.2 Total tire force coefficient 49
6.2.3 Longitudinal slip standard deviation 50
6.3 Simulations with complete system and longitudinal slip power loss based torque vectoring 52
6.3.1 Complete system with SMC 52
6.3.2 Complete system with MRAC 60
6.4 Comparison with the other cost functions 67

7 Budget **77**

8 Conclusions and future developments **79**
8.1 Conclusions 79
8.2 Future developments 80

Bibliography **85**

List of Figures

2.1 Example of 4MIDEV: Brabus Full Electric equipped with Protean Electric Motors [3] . . . 6
2.2 Exemple of an in-wheel motor by Elaphe [4] . . . 7

3.1 Vehicle model top view . . . 11
3.2 Tire model top view . . . 15
3.3 Lateral tire forces curves . . . 16
3.4 Self-aligning torques curves . . . 17
3.5 Longitudinal tire forces curves . . . 17
3.6 Motor torque curves . . . 19

5.1 General control structure . . . 34

6.1 Input curves used during simulations . . . 46
6.2 ISO double lane change test [17] . . . 46
6.3 Torque distribution of test with zero input and longitudinal slip power loss based TV . . . 48
6.4 Torque distribution of test with step input and longitudinal slip power loss based TV . . . 48
6.5 Torque distribution of test with zero input and total tire force coefficient based TV . . . 49
6.6 Torque distribution of test with step input and total tire force coefficient based TV . . . 50
6.7 Torque distribution of test with zero input and longitudinal slip standard deviation based TV . . . 51

6.8 Torque distribution of test with step input and longitudinal slip standard deviation based TV 51
6.9 Yaw rate time response with step input, SMC and longitudinal slip power loss based TV 53
6.10 Torque allocation with step input, SMC and longitudinal slip power loss based TV 54
6.11 Yaw rate time response with J-turn input, SMC and longitudinal slip power loss based TV 55
6.12 Torque allocation with J-turn input, SMC and longitudinal slip power loss based TV 56
6.13 Oscillations in yaw rate time response with J-turn input, SMC and longitudinal slip power loss based TV 56
6.14 Oscillations in torque curve with J-turn input, SMC and longitudinal slip power loss based TV 57
6.15 Yaw rate time response with single lane change input, SMC and longitudinal slip power loss based TV 58
6.16 Torque allocation with single lane change input, SMC and longitudinal slip power loss based TV 58
6.17 Yaw rate time response with double lane change input, SMC and longitudinal slip power loss based TV 59
6.18 Torque allocation with double lane change input, SMC and longitudinal slip power loss based TV 60
6.19 Yaw rate time response with step input, MRAC and longitudinal slip power loss based TV 61
6.20 Torque allocation with step input, MRAC and longitudinal slip power loss based TV 62
6.21 Yaw rate time response with ramp input, MRAC and longitudinal slip power loss based TV 63
6.22 Torque allocation with ramp input, MRAC and longitudinal slip power loss based TV 63
6.23 Yaw rate time response with J-turn input, MRAC and longitudinal slip power loss based TV 64

6.24 Torque allocation with ramp J-turn input, MRAC and longitudinal slip power loss based TV 64
6.25 Yaw rate time response with single lane change input, MRAC and longitudinal slip power loss based TV 65
6.26 Torque allocation with ramp single lane change input, MRAC and longitudinal slip power loss based TV 65
6.27 Yaw rate time response with double lane change input, MRAC and longitudinal slip power loss based TV 66
6.28 Torque allocation with ramp double lane change input, MRAC and longitudinal slip power loss based TV 67
6.29 Comparison between torque allocations with the three TVs, with step input and SMC 68
6.30 Comparison between torque allocations with the three TVs, with step input and MRAC 69
6.31 Comparison between torque allocations with the three TVs, with J-turn input and SMC 70
6.32 Yaw rate time response with J-turn input, SMC and longitudinal slip standard deviation based TV 70
6.33 Comparison between torque allocations with the three TVs, with J-turn input and MRAC 71
6.34 Comparison between torque allocations with the three TVs, with single lane change input and SMC 72
6.35 Yaw rate time response with single lane change input, SMC and longitudinal slip standard deviation based TV 73
6.36 Comparison between torque allocations with the three TVs, with single lane change input and MRAC 73
6.37 Comparison between torque allocations with the three TVs, with double lane change input and SMC 74
6.38 Results of simulation with step input, SMC and longitudinal slip power loss based TV 75

List of Tables

3.1 Vehicle and road parameters 13
3.2 Motor parameters 22

7.1 Cost estimation 78

Chapter 1

Introduction

Electric vehicles (EVs) represent the future of the automotive sector, both in the case of private/public transport and in sports competitions. Their success comes primarily from the new global regulations about emissions and pollution: indeed, electric vehicles are nowadays the most important alternative to combustion engine equipped vehicles. As their use is continuously increasing and spreading all around the world, researchers and companies are putting more and more effort to develop this field. Although the main issue is still the battery durability, all possible improvements are being investigated, like energy recovery, performance enhancements and safety systems. EVs can be classified according to the source of energy of the powertrain (hybrid vehicles, plug-in vehicles, etc.) and to the number, type and location of the electric motors.

Among the different types of EVs, the four in-wheel motor independent drive electric vehicle (4MIDEV) is one of the most interesting and with greatest margins of development and exploitation. It is equipped with four independent electric motors located into the empty space inside of each wheel, which implies significant changes both in the vehicle structure and in its functioning. The total independence of the motors permits consistent improvements in the stability control of the vehicle, carried out by a central electronic control unit (ECU), a fundamental component of EVs.

At the base of the realization of this project, there is the desire of exploiting the big advantages brought by in-wheel motors. First of all, under the stability point of view, EVs are easier to be controlled, thanks to the enhanced interaction between ECU and motors

with respect to conventional combustion vehicles. But the most significant improvement is the possibility of providing every wheel with a different torque, totally independent from the others. This permits to design and implement an optimal torque vectoring (TV) control. Torque vectoring is the technology that allows to enhance performances, handling and security by varying the torque distribution according to necessity. This is made possible in combustion engine vehicles by the use of mechanical differentials, and it is mostly adopted with all-wheel drive cars. Hence, it is clear that having four totally independent and electronically controlled motors gives enormous improvements to the application of TV.

For these motivations, the first objective of the project was to design and implement an optimal torque allocator, capable of working in continuous time with the main controller, from which receives the desired yaw moment. This is the key issue of the entire work: to control the lateral dynamics of a vehicle with a direct yaw moment control (DYC) and optimal torque vectoring. As widely explained later, an extreme simplification of the general scheme is the following: from the driver's input a reference yaw rate is generated, the DYC calculates the desired yaw moment and feeds the TV algorithm, which finally provides the vehicle plant with the optimal torque distribution. Hence, the second objective of the thesis was to design a yaw controller with high tracking performances and compatible with the TV.

The proposed solution results in a set of six different combinations between DYC and TV, that come from the different strategies adopted to face the problem. In fact, the torque allocation was addressed as a standard optimization problem, with three objective functions to be minimized that represent conceptually different approaches to the method. The problem was solved with gradient method, that showed to be efficient, fast and then compatible with the proposed DYC. As regards these latter, two solutions were proposed to control the vehicle yaw rate: a combined PID and sliding-mode control, and a model reference adaptive control (MRAC). Combining the three distribution methods with the two controllers, the mentioned set of six systems is obtained.

The systems were implemented in MATLAB and tested in Simulink, trying to reproduce some of the common test maneuvers, like J-turn or single and double line changes.

Results of simulations were compared to evaluate every solution in terms of tracking and torque curves, highlighting any differences, points of strength and weaknesses among them.
Satisfying results were achieved in the analyzed scenarios, with information about the possibility of application on a real vehicle and suggestions towards future enhancements and developments.

Here is a brief description of the structure and development of the thesis.
Chapter 2 deals with the state of the art of the treated arguments. It includes a general summary on the in-wheel technology and 4MIDEVs, and a description of previous works done on torque vectoring, torque distribution criteria and direct yaw moment control.
Chapters 3, 4 and 5 represent the theoretical part of the thesis, in which the realized work is developed and explained in details. In Chapter 3 the vehicle model is presented in all its relevant features and all the hypotheses and assumptions taken are defined. Chapter 4 deals with the torque vectoring process, defining the problem, formulating the three cost function adopted and explaining the functioning of gradient method. In Chapter 5 the yaw control is treated, starting from the general prerequisites of the controller and ending with the description of the proposed solutions.
In Chapter 6 all the previously designed solutions are tested through simulations in Simulink, the results are graphically shown and critically commented emphasizing key characteristics.
Finally, conclusions and possible future developments are treated in Chapter 8.

Chapter 2

State of the art

2.1 The 4MIDEV

Among the various kind of electric vehicles developed nowadays, the 4MIDEV is one of the most peculiar. The idea of placing the motors in the inner empty space of the wheels it is not new: in 1900 Ferdinand Porsche presented the first in-wheel electric vehicle, the "System Lohner-Porsche". It was driven by two in-wheel electric motors and capable of reaching over 55km/h. During the following years, the vehicle was equipped with a combustion engine too, creating the first hybrid vehicle of the history [1].

Anyway, in the 20th century combustion engines became undoubtedly the most common technology for tourism vehicles; even though electric vehicles continued their development, in-wheel technology was partly discarded due to its dynamical disadvantages. Indeed, one of the most relevant differences between in-wheel and traditional vehicles is the effect of the weight of the motors inside the wheels, which produces an increment of at least 30kg of unsprung masses at each motor equipped wheel. At the beginning of last century, with the technology of the time, those unsprung masses were difficultly handled in common tourism vehicle, but nowadays, with the enormous development in terms of suspensions, in-wheel electric vehicles are coming back as one of the most interesting and exploitable solutions.
Recent studies showed that the increment in unsprung mass can be compensated by common chassis with acceptable driving comfort; performances could be enhanced with

Figure 2.1: Example of 4MIDEV: Brabus Full Electric equipped with Protean Electric Motors [3]

specific chassis design and tires [2].

Besides the mentioned drawbacks, there are a lot of enhancements that could be obtained with the installation of in-wheel motors. First of all, many typical components of a classic vehicles can be removed as they get useless: they include external gearboxes, drivetrains, half-shafts, axles and differentials. This implies substantial mechanical simplifications, with considerable reduction of power losses, and gives the designer greater flexibility. All these components are usually substituted by a single-speed in-wheel transmission [3].

Beyond the mechanical simplifications, the most valuable advantages deal with the electronic stability control of the vehicle: indeed, the motors are totally independent among each others, and the controller can provide each of them with different torque. This is the basis of the application of torque vectoring, which is treated in the following section. Launch control and traction control can be easily improved as well.

According to Elaphe and Protean Electric, which are some of the most important in-wheel motor producers, motor power can reach up to 100kW, with peak torques up to 1400Nm. These values concern a single motor, if the vehicle is a 4MIDEV it means that the overall performances are produced by the combination of four motors. Furthermore, many motors include a regenerative braking system, which recovers the kinetic energy to store it or to make it immediately available [3, 4].

Figure 2.2: Exemple of an in-wheel motor by Elaphe [4]

2.2 Torque vectoring control

The natural consequence of equipping a vehicle with four independent in-wheel motors is the design of an optimal torque vectoring control, to improve stability and performances of the vehicle. Torque vectoring was at first applied to combustion engine vehicles, where torques were distributed to the wheels through mechanical differentials. It started to become popular with all-wheel drive vehicles, because of the extended possibilities of torque allocation with respect to a front/rear wheel drive vehicle. But the most relevant achievements started with the spread of electric vehicles.

The main issue is the criterion on which the torque vectoring is based, since there are many ways of optimizing the distribution. A comparison between different criteria for a all-wheel drive combustion vehicle is presented in [5]. Four objective functions are analyzed: total power loss, longitudinal slip power loss, longitudinal slip standard deviation and average combined tire force coefficient. Here, the torque computation is realized offline with an iterative method.

A multi-objective based optimization, instead, is presented in [6]. In this paper, the cost function is a combination of yaw moment control offset, drive energy loss and tire slip restrictions, and both offline and online optimizations are treated.

A further step is the combination of torque vectoring with direct yaw moment control, which governs vehicle stability. In [7], the authors designed yaw moment controller with combined feedback and feedforward contribution, actuated with the electric drivatrains and friction brakes.

In the case of a 4MIDEV, the friction brakes can be substituted by the braking torques of the in-wheel motors. This is a full exploitation of the torque vectoring possibilities, that now is in charge of all the vehicle stability. An example of this kind of solution is treated in [8]: a stability control is proposed with a fuzzy yaw moment controller and total tire force based torque distribution; the system is enriched with a fuzzy tire slip control and a stability judgment algorithm that activates the main controller.

In this thesis, sliding mode and MRAC are implemented for the direct yaw moment control. An integral sliding mode control, combined with torque vectoring, is proposed in [9]: the system was validated with simulations in CarMaker and then with experimental assessment; sliding model control showed good performances, even taking into account the communication delays in the signal transmission. In this paper, the connection between yaw moment control and torque vectoring is not analyzed in detail, as well as the optimization itself which is not present.

As for MRAC, an adaptive direct yaw model control is developed in [10]. The idea is that the yaw moment model adopted to generate the yaw rate reference always implies uncertainties and errors due to approximations. With a yaw moment model identification and an adaptive control law based on it, enhancements in the yaw rate tracking were achieved with respect to the nominal system without estimation.

Chapter 3

Model

In absence of a real vehicle or a specific simulator, a tourism vehicle with standard dimensions and parameters was modeled under these hypotheses: it is a 4MIDEV, so the four electric motors occupy the empty spaces inside of each wheel; the batteries are collocated in the front part, where there is usually the combustion engine, so the center of gravity is closer to the front axle; the vertical dynamics (suspensions and weight transfers) are neglected: the weight is equally distributed between left and right wheels, and divided between front and rear just solving a moment equilibrium with respect to the center of gravity. The adopted values are listed in Table 3.1

In the sections below, longitudinal dynamics, non-linear and linearized lateral dynamics, tire model and electric motors characteristics are presented.

3.1 Vehicle dynamics model

A vehicle dynamics model is needed to express the behavior of the vehicle in response of the driver's input variables. The pressures on the throttle and brake pedals give the demanded drive and brake forces, which combined with the steering angle feed the electronic control to generate the four wheel torques. These torques and the steering angle are the input variables of the vehicle model. The output variables are the yaw rate and the side-slip angle of the vehicle. It is possible to split the dynamics into two sub-models: the longitudinal dynamics, which deals with the movement of the vehicle along its longitudinal

axis, and the lateral dynamics, which includes the lateral displacement and the yaw rotation.

3.1.1 Longitudinal dynamics

The development of this model starts from taking a lateral view of the vehicle in movement and highlighting the forces that act on it [11]. These are: the weight force, calculated as $mg\sin\theta$, where θ is the road's inclination angle, the aerodynamic drag force F_{aero}, the longitudinal drive forces F_{xf} and F_{xr}, respectively at the front and rear tires, the rolling resistance forces R_{xf} and F_{xr}, respectively at the front and rear tires, and the inertia force calculated as $m\ddot{x}$, being $\ddot{x}$ the longitudinal acceleration of the car.
Writing the equilibrium equation along the x direction one gets:

$$m\ddot{x} = F_{xf} + F_{xr} - F_{aero} - R_{xf} - R_{xr} - mg\sin\theta. \tag{3.1}$$

The aerodynamic drag force can be expressed as:

$$F_{aero} = \frac{1}{2}\rho C_d A_F (V_x + V_{wind})^2 \tag{3.2}$$

where ρ is the density of air, C_d is the aerodynamic drag coefficient, A_F is the frontal area of the vehicle, $V_x = \dot{x}$ is the longitudinal speed, V_{wind} is the wind velocity.
In standard conditions (sea level altitude, barometric pressure of 101.32kPa and 15°C) ρ can be taken as 1.255kg/m^3. C_d is in the range of 0.25÷0.3 for a modern tourism car. A_F is the projection of the vehicle's area on a plane perpendicular to the travel direction; for a passenger car with mass in the range of 800÷2000kg it can be calculated with the formula:

$$A_F = 1.6 + 0.00056(m - 765). \tag{3.3}$$

The sign of the wind velocity V_{wind} is positive for headwind and negative for tailwind; at ground level it can often be taken as zero.

The terms F_{xf} and F_{xr} represent respectively the overall front and rear longitudinal tire forces, they are the result of the interaction between the ground and the tires; their formulation will be explained in section 3.1.3.

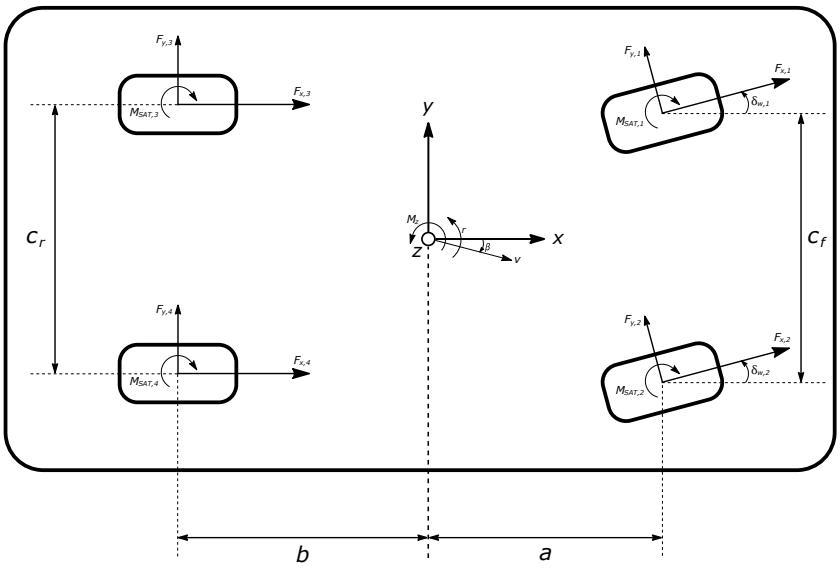

Figure 3.1: Vehicle model top view

The rolling resistance is the effect of the tire's deformation caused by the contact with the ground. Due to the material's damping, the energy spent deforming the tire is not completely recovered and this loss is represented by a force applied to the tire that opposes to the longitudinal motion of the vehicle. It is generally calculated by multiplying the vertical force on each tire times the rolling resistance coefficient f, hence:

$$R_{xf} + R_{xr} = f(F_{zf} + F_{zr}), \tag{3.4}$$

being F_{zf} and F_{zr} respectively the vertical forces acting on the front and rear wheels. For a car tire traveling on asphalt the value of f usually stays in the range of $0.01 \div 0.02$.

3.1.2 Lateral dynamics

The rotation of the vehicle among its z axis, known as yaw, is a fundamental indicator of the vehicle conditions. Starting from the top view of the vehicle in Fig. 3.1 a yaw moment balance at the center of mass is performed, taking in consideration for each tire the longitudinal force F_x, the lateral force F_x and the self-aligning torque M_{SAT} [11, 12]. These three parameters are evaluated with the Pacejka's magic formula from the side-slip angle β and the slip ratio σ_x. The position of the center of mass is supposed to be known

and constant.The resulting equation is:

$$\begin{aligned} J_z\dot{r} = (-F_{x,1}\cos\delta_{w,1} + F_{y,1}\sin\delta_{w,1} + F_{x,2}\cos\delta_{w,2} - F_{y,2}\sin\delta_{w,2})\,\frac{c_f}{2} + \\ + (F_{x,1}\sin\delta_{w,1} + F_{y,1}\cos\delta_{w,1} + F_{x,2}\sin\delta_{w,2} + F_{y,2}\cos\delta_{w,2})\,a + \\ + (-F_{x,3} + F_{x,4})\,\frac{c_r}{2} - (F_{y,3} + F_{y,4})\,b - M_{SAT,1} - M_{SAT,2} - M_{SAT,3} - M_{SAT,4}, \end{aligned} \tag{3.5}$$

where $\dot{r}$ is the yaw acceleration (being r the yaw rate), $\delta_{w,1}$ and $\delta_{w,2}$ are, respectively, the left and right steer angles, c_f and c_r are, respectively, the front and rear track widths, a and b are the distances from the center of gravity of the front and rear tracks respectively.

The second equation comes from the lateral dynamics analysis, expressed as the displacement of the center of mass along the y vehicle's axis. The resulting equation is the following:

$$mV_x(\dot{\beta} + r) = F_{y,1}\cos\delta_{w,1} + F_{y,2}\cos\delta_{w,2} + F_{y,3} + F_{y,4} + F_{x,1}\sin\delta_{w,1} + F_{x,2}\sin\delta_{w,2} \tag{3.6}$$

where m is the total mass and u_x is the speed of the center of mass along the longitudinal vehicle's axis. The lateral forces F_y and self-aligning torques M_{SAT} are calculated with the Pacejka's Magic Formula, explained in detail in the following section.

Symbol	Description	Value
m	vehicle mass	1410kg
J_z	moment of inertia about z axis	2030kgm^3
R	tire radius	0.3 m
a	distance between center of gravity and front axle	1.04m
b	distance between center of gravity and rear axle	1.56m
c_f	front axle width	1.48m
c_r	rear axle width	1.48m
$C_{\alpha,f}$	front tires cornering stiffness	20450N/rad
$C_{\alpha,r}$	rear tires cornering stiffness	17724N/rad
$C_{M,f}$	front tires self-aligning torque stiffness	855Nm/rad
$C_{M,r}$	rear tires self-aligning torque stiffness	550Nm/rad
$C_{\sigma_x,f}$	front tires longitudinal stiffness	828N
$C_{\sigma_x,r}$	rear tires longitudinal stiffness	549N
μ	friction coefficient	0.7
f	rolling resistance	0.015

Table 3.1: Vehicle and road parameters

3.1.3 Tire model: the Pacejka's Magic Formula

The Pacejka's tire model allows to calculate the forces and moments acting on a rotating wheel as harmonic functions of the slip ratios (lateral or longitudinal). The name comes from the fact that the formulas do not have any physical bases but they are mathematical expressions derived from experimental analysis.

Considering a single rolling tire, F_y and M_{SAT} generate only when cornering: in fact, in this situation the tire slips laterally on the ground, the slip angle α is the angle formed between the actual velocity of the wheel and its rolling direction. This condition generates the lateral force F_y, which is applied slightly behind the center of the wheel and so produces the self-aligning torque M_{SAT}. These forces also depend on the normal force applied to the wheel and on the camber angle, if present, that combined with a series of experimental coefficients give the formulas in their final form [11, 12, 13]:

$$F_y = D\sin(C\arctan(B\varphi)) + S_v \tag{3.7}$$

$$M_{SAT} = D\sin(C\arctan(B\varphi)) + S_v \tag{3.8}$$

$$F_x = D\sin(C\arctan(B\varphi)) \tag{3.9}$$

where B, C, D are different for every equation, they are functions of F_z and other specific coefficients for every force calculated; φ is a function of the side-slip angle α for the cases of F_y and M_{SAT}, and a function of the longitudinal percent slip σ_x for the case of F_x; S_v is the correction factor that takes in consideration the presence of the camber angle.

The front and rear side-slip angles α_f and α_r are defined as:

$$\alpha_f = \delta - \theta_f \tag{3.10}$$

$$\alpha_r = -\theta_r, \tag{3.11}$$

where δ is the tire steer angle, θ_f and θ_r are respectively the angles that the front tires' velocity vector and the rear tires velocity vector make with the longitudinal axis. They can be calculated as:

$$\theta_f = \beta + \frac{ar}{V_x} \tag{3.12}$$

$$\theta_r = \beta - \frac{br}{V_x} \tag{3.13}$$

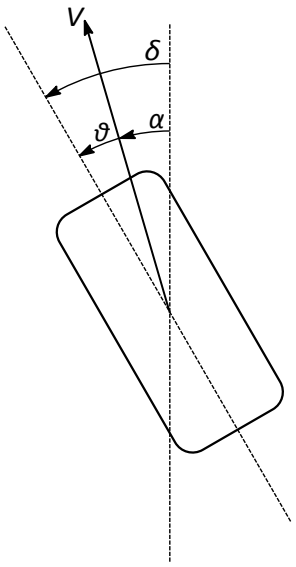

Figure 3.2: Tire model top view

being β,a,b,r and V_x the quantities defined in the previous sections.

The longitudinal slip σ_x is defined as the ratio between the longitudinal slip and the longitudinal velocity at the wheel axle. The longitudinal slip is the difference between the rotational velocity and the actual longitudinal velocity $\omega_w R - V_x$; hence:

$$\sigma_x = \frac{\omega_w R - V_x}{V_x} \tag{3.14}$$

during acceleration, and

$$\sigma_x = \frac{\omega_w R - V_x}{\omega_w R} \tag{3.15}$$

during braking.

For small values of α ($-5 \div 5$deg), F_y can be approximated as a linear function of the slip angle; it yields:

$$F_y = C_\alpha \alpha. \tag{3.16}$$

C_α is called the lateral cornering stiffness of the tire. Same considerations could be made for the longitudinal force, with a percent slip in the range of $-5 \div 5$:

$$F_x = C_{\sigma_x} \sigma_x. \tag{3.17}$$

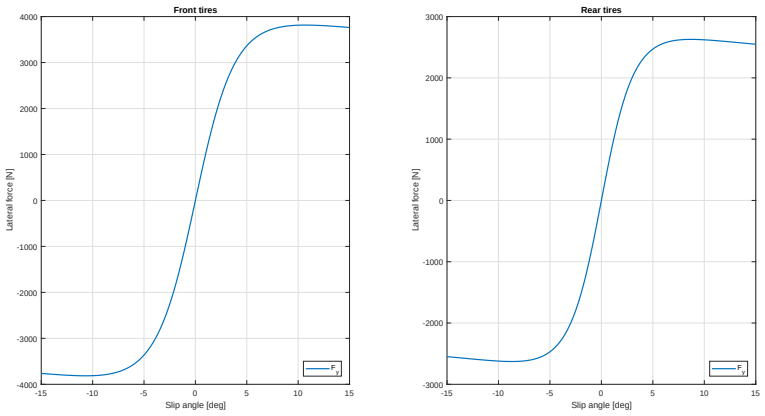

Figure 3.3: Lateral tire forces curves

so C_{σ_x} is the longitudinal tire stiffness.

Finally, also M_{SAT} could be assumed as a linear function of α, but for very small values of the angle ($-2 \div 2$deg).

Another way to express the longitudinal force F_x is to write the equilibrium equation along the x axis of the wheel: in this way the effect of the applied torque is emphasized. It yields:

$$\frac{T_w}{R} - \frac{T_b}{R} - F_x - f_r F_z = m a_x. \tag{3.18}$$

The $f_r F_z$ term can often be neglected, and in case of constant speed hypothesis one gets:

$$F_x = \frac{T_w - T_b}{R}. \tag{3.19}$$

The curves obtained with the Pacejka's Formula are shown in Fig. 3.3, 3.4 and 3.5.

3.1.4 State-space model

Under certain conditions a simplified state-space model for the lateral dynamics can be developed. Under the hypothesis of small slip angles it is possible to use de linear expressions of F_y and M_{SAT}. As regards F_x, assuming V_x constant and neglecting the rolling

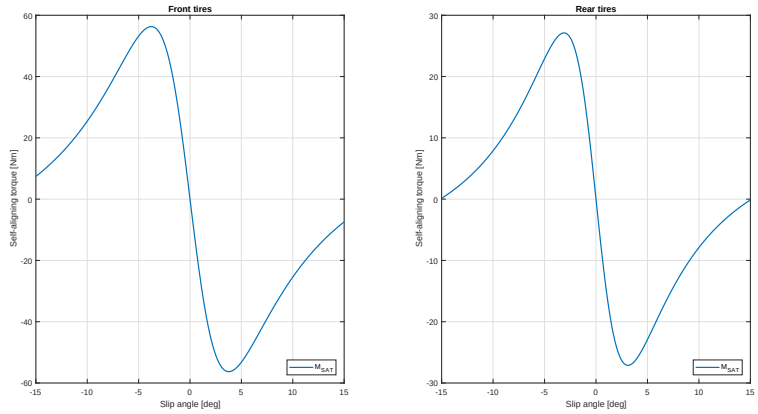

Figure 3.4: Self-aligning torques curves

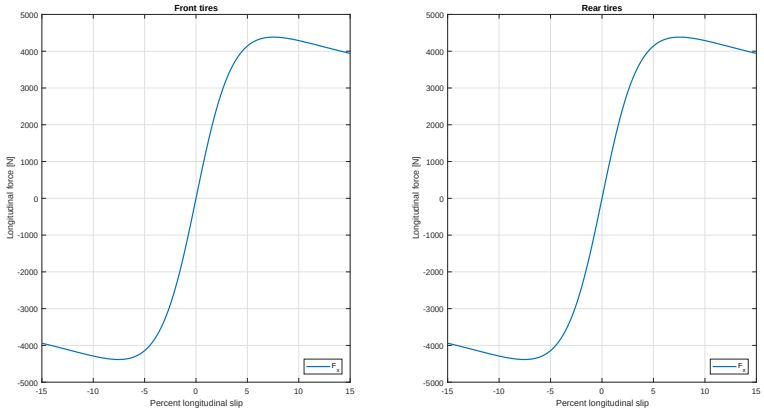

Figure 3.5: Longitudinal tire forces curves

resistance terms R_x, it becomes:

$$F_{x,i} = \frac{T_i}{R}, \tag{3.20}$$

where T_i is the overall torque (drive minus braking) that each wheel receives from the motor. Finally a mean value for the steering angle is adopted:

$$\delta = \frac{\delta_{w,1} + \delta_{w,2}}{2}. \tag{3.21}$$

Applying these simplifications to the model described by (3.5) and (3.6), one gets:

$$\begin{cases} \dot{r} = \left[\frac{2\left(-a^2 C_{\alpha_f} - b^2 C_{\alpha_r} + aC_{Mf} - bC_{Mr}\right)}{J_z V_x}\right] r + \left[\frac{2\left(-aC_{\alpha_f} + bC_{\alpha_r} + C_{Mf} + C_{Mr}\right)}{J_z}\right] \beta + \\ + \left[\frac{2\left(aC_{\alpha_f}\cos\delta - C_{Mf}\right)}{J_z}\right] \delta + \left(\frac{a\sin\delta - \frac{c_f}{2}\cos\delta}{RJ_z}\right) T_1 + \left(\frac{a\sin\delta + \frac{c_f}{2}\cos\delta}{RJ_z}\right) T_2 + \\ - \left(\frac{c_r}{2RJ_z}\right) T_3 + \left(\frac{c_r}{2RJ_z}\right) T_4 \\ \\ \dot{\beta} = \left[\frac{2\left(bC_{\alpha_r} - aC_{\alpha_f}\right)}{mV_x^2} - 1\right] r + \left[\frac{-2\left(C_{\alpha_f} + C_{\alpha_r}\right)}{mV_x}\right] \beta + \left(\frac{2C_{\alpha_f}\cos\delta}{mV_x}\right) \delta + \\ + \left(\frac{\sin\delta}{mRV_x}\right) T_1 + \left(\frac{\sin\delta}{mRV_x}\right) T_2. \end{cases} \tag{3.22}$$

The system can be rewritten in the standard state-space form $\dot{\mathbf{x}} = \mathbf{A}\mathbf{x} + \mathbf{B}\mathbf{u} + \mathbf{E}\delta$, being:

$$\mathbf{x} = \begin{bmatrix} r \\ \beta \end{bmatrix}; \mathbf{u} = \begin{bmatrix} T_1 \\ T_2 \\ T_3 \\ T_4 \end{bmatrix}.$$

The system is non-linear due to the presence of $\cos\delta$ and $\sin\delta$ in $\mathbf{B}$, however since δ is usually very small a further linearization can be applied, i.e. $\cos\delta \approx 1$ and $\sin\delta \approx \delta$. Hence, the $\mathbf{A}$, $\mathbf{B}$ and $\mathbf{E}$ matrices are [11, 12]:

$$\mathbf{A} = \begin{bmatrix} \frac{2\left(-a^2C_{\alpha_f} - b^2C_{\alpha_r} + aC_{Mf} - bC_{Mr}\right)}{J_z V_x} & \frac{2\left(-aC_{\alpha_f} + bC_{\alpha_r} + C_{Mf} + C_{Mr}\right)}{J_z} \\ \frac{2\left(-aC_{\alpha_f} + bC_{\alpha_r}\right)}{mV_x^2} - 1 & \frac{-2\left(C_{\alpha_f} + C_{\alpha_r}\right)}{mV_x} \end{bmatrix} \tag{3.23}$$

$$\mathbf{B} = \begin{bmatrix} \frac{a\delta - \frac{c_f}{2}}{RJ_z} & \frac{a\delta + \frac{c_f}{2}}{RJ_z} & -\frac{c_r}{2RJ_z} & \frac{c_r}{2RJ_z} \\ \frac{\delta}{mRV_x} & \frac{\delta}{mRV_x} & 0 & 0 \end{bmatrix} \tag{3.24}$$

$$\mathbf{E} = \begin{bmatrix} \frac{2\left(aC_{\alpha_f} - C_{Mf}\right)}{J_z} \\ \frac{2C_{\alpha_f}}{mV_x} \end{bmatrix} \tag{3.25}$$

A key issue is the fact that δ is not part of the control action $\mathbf{u}$ but is treated separately as a disturbance: indeed, it is directly controlled by the driver with the steering wheel, but from the controlled system's point of view it must be considered as an external uncontrolled perturbation.

3.2 Electric motors

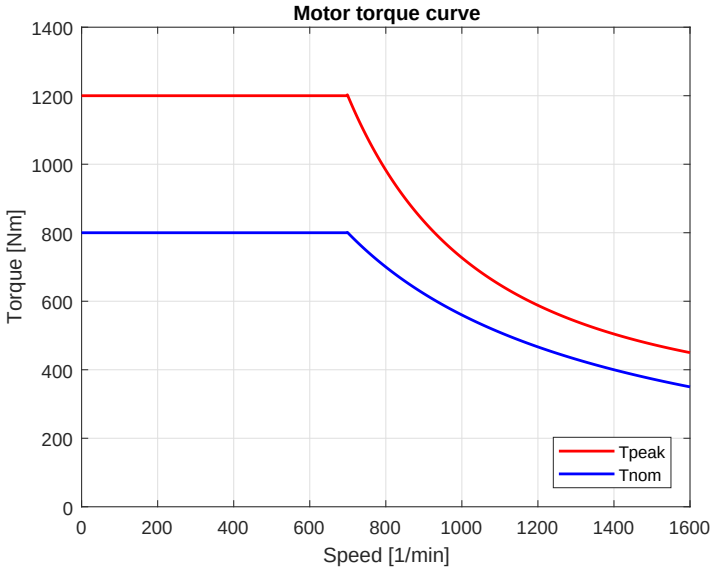

Figure 3.6: Motor torque curves

As for the case of the general vehicle model, the electric motors used are not real commercial products, but hypothetical components obviously with performances and characteristics consistent with the existing technology.
In this work, the most relevant characteristic of the motors is the torque curve, that represents the physical limitation to the torque optimizer. The general torque vs rotational speed curve of an in-wheel induction motor is shown in Fig 3.6. The red curve is the peak torque, the maximum torque that the motor can produce for a short period of time, while the blue curve represents the rated (or nominal) torque, that is the torque that the motor can produce at a determined rated speed for an unlimited time. First of all, even if it is not showed in the picture, it is reasonable to suppose that the motor behaves in the same way both in drive and brake mode (positive or negative torques). The curve can be split into two main zones: the first one is the constant torque zone, in which the curve is constant at its maximum T_{max}; this zone ends when the motor reaches a determinate rotational speed $\omega_{m,0}$; from this value, the motor is working at its maximum power, both peak and rated torques start decreasing until the maximum speed is reached. The rated torque can be calculated as

$$T_{m,nom}(\omega_m) = \frac{P_{nom}\eta}{\omega_m} \tag{3.26}$$

where P_{nom} is the nominal power and η is the motor efficiency. The peak torque instead decreases faster with a trend proportional to inverse of the squared rotational speed.

$$T_{m,peak}(\omega_m) \propto \frac{1}{\omega_m^2} \tag{3.27}$$

3.3 Introduction to control objectives

Once a dynamics model is adopted the focus shifts on the system's control strategy. As said, the inputs of the model are the steer angle and the wheel torques: the first one comes directly from the driver, while the latter are the result of different control blocks. These are the core of the project and they will be developed in details in the following chapters. The general objective is to ensure a correct trajectory tracking at cornering, with a stable behavior of the vehicle and robust response in case of disturbances. Here follows an introductory analysis of the various controllers, highlighting inputs, outputs and objectives of each of them.

3.3.1 Yaw moment controller

The first part of the control system deals with the tracking of the car's yaw rate: when the driver starts a cornering maneuver the vehicle should follow a specific path, which implies the creation of a reference value for the yaw rate. Specifically, this value is the ratio between the longitudinal speed V_x and the radius of curvature of the desired trajectory R:

$$r_{des} = \frac{V_x}{R}. \tag{3.28}$$

The curvature radius can be expressed as a function of the steering angle δ applied by the driver to face the cornering; one gets:

$$r_{des} = \frac{V_x}{L + \frac{mV_x^2(aC_{\alpha f} - bC_{\alpha r})}{2C_{\alpha f}C_{\alpha r}L}}\delta, \tag{3.29}$$

where $L = a + b$ is the total wheelbase of the vehicle, $C_{\alpha f}$ and $C_{\alpha r}$ are, respectively, the front and rear cornering stiffnesses of the wheels, as in Chapter 8 of [11].
The desired yaw rate is the input to the yaw moment controller, while the output is the required yaw moment $M_{z,des}$, which in turn will be one of the inputs of the following control block.

3.3.2 Torque vectoring

Once the yaw moment reference $M_{z,des}$ is generated, the following step is to combine it with the total drive/brake force that comes from the driver's action in order to feed the torque vectoring controller. The total drive/brake force comes from the conversion of the throttle and brake pedals' pressures into a reference value for the longitudinal force F_x. Hence, the torque vectoring has the function of finding the optimal distribution of the total drive force to the four wheels, since in a 4MIDEV a different torque can be applied to each wheel. The main idea is to use a minimum objective function optimization, with some limitations added to avoid tire slipping and obviously to generate torques that could actually be produced by the motors. Those will be the restrictions to the objective function. Hence, the output of this stage is a vector containing the four torques that have to be given to the wheels; with this source the vehicle model is fed and through the drivetrain model the demanded torques at the motors are calculated.

Symbol	Description	Value
P_{max}	rated power	80kW
P_{nom}	rated power	60kW
T_{peak}	peak torque	1200Nm
T_{nom}	rated torque	800Nm
$\omega_{m,0}$	rated rotational speed	700rpm
$\omega_{m,max}$	maximum rotational speed	1600rpm
η	motor efficiency	0.95

Table 3.2: Motor parameters

Chapter 4

Torque vectoring

There are many ways to approach torque allocation. In this thesis all the different methods considered include the resolution of a constrained minimum objective function problem, and the difference between them concerns the function to minimize. The objective functions analyzed and tested in this project are: the power loss due to longitudinal tire slip, the total tire force coefficient and the longitudinal slip standard deviation [5].
In the following sections each objective function is explained and a formulation of the problem is provided, but first it is necessary to define the restrictions of the optimization problem, that will be the same for all the cost functions.

4.1 Restrictions

As previously said, the functions are constrained by the desired $M_{z,des}$ and $F_{x_{TOT},des}$ and by the physical limitations regarding the torques.
The first two restrictions come from the dynamics of the vehicle. The sum of the four longitudinal forces generated by the resulting torques must be equal to the total desired drive force coming from the longitudinal dynamics:

$$F_{x_{TOT},des} = F_{x_1} + F_{x_2} + F_{x_3} + F_{x_4}. \tag{4.1}$$

Applying (4.25) and rewriting in vectorial form it yields:

$$F_{x_{TOT},des} = \mathbf{b}_1 \mathbf{T}, \tag{4.2}$$

being

$$\mathbf{b}_1 = \begin{bmatrix} \frac{1}{R} & \frac{1}{R} & \frac{1}{R} & \frac{1}{R} \end{bmatrix}.$$

The second restriction is the one generated by the control action $M_{z,des}$. Starting from the yaw moment balance:

$$\begin{aligned} M_{z,des} = &\left(-F_{x,1}\cos\delta_{w,1} + F_{y,1}\sin\delta_{w,1} + F_{x,2}\cos\delta_{w,2} - F_{y,2}\sin\delta_{w,2}\right)\frac{c_f}{2} + \\ &+ \left(F_{x,1}\sin\delta_{w,1} + F_{y,1}\cos\delta_{w,1} + F_{x,2}\sin\delta_{w,2} + F_{y,2}\cos\delta_{w,2}\right)a + \\ &+ \left(-F_{x,3} + F_{x,4}\right)\frac{c_r}{2} - \left(F_{y,3} + F_{y,4}\right)b - M_{SAT,1} - M_{SAT,2} - M_{SAT,3} - M_{SAT,4}, \end{aligned} \tag{4.3}$$

it is possible to split the terms on the right side according to the type of force they come from, i.e. F_x, F_y or M_{SAT}:

$$M_{z,des} = M_{z,x} + M_{z,y} + M_{z,SATs}. \tag{4.4}$$

Since the controllable terms are the ones depending on F_x while the others are known from the vehicle model, the focus is set on the yaw moment generated by longitudinal forces:

$$M_{z,x,des} = M_{z,des} - M_{z,y} - M_{z,SATs}, \tag{4.5}$$

which leads to:

$$M_{z,x,des} = \left(a\sin\delta - \frac{c_f}{2}\cos\delta\right)F_{x_1} + \left(a\sin\delta + \frac{c_f}{2}\cos\delta\right)F_{x_2} - \frac{c_r}{2}F_{x_3} + \frac{c_r}{2}F_{x_4}. \tag{4.6}$$

Also in this case the simplification of (3.21) about the mean steering angle has been adopted. The final vectorial form is:

$$M_{z,x,des} = \mathbf{b}_2\mathbf{T} \tag{4.7}$$

where

$$\mathbf{b}_2 = \begin{bmatrix} \frac{a\sin\delta - \frac{c_f}{2}\cos\delta}{R} & \frac{a\sin\delta + \frac{c_f}{2}\cos\delta}{R} & -\frac{c_r}{2R} & \frac{c_r}{2R} \end{bmatrix}.$$

Finally, it is possible to incorporate these first two constraints in a single equation.

$$\mathbf{B}_{TV}\mathbf{T} - \mathbf{c} = 0 \tag{4.8}$$

where $\mathbf{c}$ and $\mathbf{B}_{TV}$ are built as:

$$\mathbf{c} = \begin{bmatrix} F_{x_{TOT},des} \\ M_{z,x,des} \end{bmatrix}; \mathbf{B}_{TV} = \begin{bmatrix} \mathbf{b}_1 \\ \mathbf{b}_2 \end{bmatrix}.$$

Let us consider now the physical constraints that limit the torques. There are three factors that contribute to generate the restriction: the maximum torque that can be produced by the motors, the road adhesion equation and the friction circle equation. Since these values can change they are all calculated at every instant and the restriction is represented by the most limiting one.
The four in-wheel motors are supposed to be all the same, thus the restrictions to the four wheels will be identical. Supposing that the system reaches saturation for very short times, it is possible to take the peak torque as the limit; if this hypothesis resulted not to be valid during simulations, it would be discarded and nominal torque would be used. Following Section 3.2 the constraint, evaluated at the wheels, is:

$$|T_{max,w,i}| = \begin{cases} \frac{T_{m,peak}\eta}{i}, & \text{if} \quad 0 \leq \omega_w < \omega_{w,0} \\ \frac{P_{max}\eta}{\omega_w^2}, & \text{if} \quad \omega_{w,0} \leq \omega_w \leq \omega_{w,max}. \end{cases} \tag{4.9}$$

The second constraint comes from the road adhesion coefficient, i.e.:

$$|T_{max,ad,i}| = \mu_{x_i} F_{z_i} R \tag{4.10}$$

being μ_{x_i} the longitudinal friction coefficient.

The last restriction is the one arising from the compliance of the friction circle equation, which is:

$$\left(\frac{F_{x_i}}{F_{x,max}}\right)^2 + \left(\frac{F_{y_i}}{F_{y,max}}\right)^2 \leq 1. \tag{4.11}$$

The maximum longitudinal and lateral forces can be defined as

$$F_{x,max} = \mu_{x_i} F_{z_i} \tag{4.12}$$

$$F_{y,max} = \mu_{y_i} F_{z_i} \tag{4.13}$$

and including (4.25) the final limit expression is:

$$|T_{max,fr,i}| = R\mu_{x_i} F_{z_i} \sqrt{\left(1 - \left(\frac{F_{y_i}}{\mu_{y_i} F_{z_i}}\right)^2\right)}. \tag{4.14}$$

Combining all the relationships it is possible to write the overall condition as:

$$|T_i| \leq \min\left(T_{max,w,i}, T_{max,ad,i}, T_{max,fr,i}\right). \tag{4.15}$$

In the vector form, it is

$$\mathbf{T}_{min} \leq \mathbf{T} \leq \mathbf{T}_{max}. \tag{4.16}$$

4.2 Cost functions

4.2.1 Longitudinal slip power loss

The first approach to write the cost function of the minimization problem is the one that aims at reducing the power losses due to longitudinal tire slip. The objective function can be written as follows [5]:

$$J = \min_{\mathbf{T}} \sum_{i=1}^{4} \left|F_{x_i} V_{s,x_i}\right|, \tag{4.17}$$

where V_{s,x_i} is the longitudinal slip velocity of each wheel, which can be also expressed as

$$V_{s,x_i} = V_{w,i}\sigma_{x_i}, \tag{4.18}$$

being $V_{w,i}$ the velocity at the center of the wheel. As before, using (3.17) and (4.25) one gets:

$$J = \min_{\mathbf{T}} \sum_{i=1}^{4} \frac{T_i^2 V_{w,i}}{R^2 C_{\sigma_i}}. \tag{4.19}$$

Defining the matrix $\mathbf{D}$ as

$$\mathbf{D} = \begin{bmatrix} \frac{V_{w,1}}{R^2 C_{\sigma_1}} & 0 & 0 & 0 \\ 0 & \frac{V_{w,2}}{R^2 C_{\sigma_2}} & 0 & 0 \\ 0 & 0 & \frac{V_{w,3}}{R^2 C_{\sigma_3}} & 0 \\ 0 & 0 & 0 & \frac{V_{w,4}}{R^2 C_{\sigma_4}} \end{bmatrix},$$

the final expression is:

$$\min_{\mathbf{T}} \quad J = \mathbf{T}^T \mathbf{D} \mathbf{T} \tag{4.20}$$

$$s.t. \quad \mathbf{B}_{TV}\mathbf{T} - \mathbf{c} = 0 \tag{4.21}$$

$$\mathbf{T} - \mathbf{T}_{min} \geq 0 \tag{4.22}$$

$$\mathbf{T}_{max} - \mathbf{T} \geq 0 \tag{4.23}$$

4.2.2 Total tire force coefficient

In this second case the objective function to minimize is the total tire force coefficient, defined as [5]:

$$J = \min_{\mathbf{T}} \sum_{i=1}^{4} \frac{\sqrt{F_{x_i}^2 + F_{y_i}^2}}{F_{z_i}}. \tag{4.24}$$

Considering the most simplified tire model presented in Section 3.1.3, each wheel's longitudinal force can be expressed as a function of the applied torque:

$$F_{x_i} = \frac{T_i}{R}. \tag{4.25}$$

A vector expression of the objective function is needed in order to apply any type of solver, so the following vectors and matrices are defined:

$$\mathbf{T} = \begin{bmatrix} T_1 \\ T_2 \\ T_3 \\ T_4 \end{bmatrix}; \mathbf{Y} = \begin{bmatrix} F_{y_1} \\ F_{y_2} \\ F_{y_3} \\ F_{y_4} \end{bmatrix}; \mathbf{Z}^T = \begin{bmatrix} \frac{1}{F_{z_1}} \\ \frac{1}{F_{z_2}} \\ \frac{1}{F_{z_3}} \\ \frac{1}{F_{z_4}} \end{bmatrix};$$

$$\mathbf{X} = \begin{bmatrix} T_1 & 0 & 0 & 0 \\ 0 & T_2 & 0 & 0 \\ 0 & 0 & T_3 & 0 \\ 0 & 0 & 0 & T_4 \end{bmatrix}; \mathbf{W} = \begin{bmatrix} F_{y_1} & 0 & 0 & 0 \\ 0 & F_{y_2} & 0 & 0 \\ 0 & 0 & F_{y_3} & 0 \\ 0 & 0 & 0 & F_{y_4} \end{bmatrix}.$$

Thus, the objective function can be rewritten as:

$$J = \min_{\mathbf{T}} \mathbf{Z} \left(\frac{1}{R^2} \mathbf{X}\mathbf{T} + \mathbf{W}\mathbf{Y} \right)^{\frac{1}{2}} \tag{4.26}$$

The complete formulation of the problem is:

$$\min_{\mathbf{T}} \quad J = \mathbf{Z}\left(\frac{1}{R^2}\mathbf{X}\mathbf{T} + \mathbf{W}\mathbf{Y}\right)^{\frac{1}{2}} \tag{4.27}$$

$$\text{s.t.} \quad \mathbf{B}_{TV}\mathbf{T} - \mathbf{c} = 0 \tag{4.28}$$

$$\mathbf{T} - \mathbf{T}_{min} \geq 0 \tag{4.29}$$

$$\mathbf{T}_{max} - \mathbf{T} \geq 0 \tag{4.30}$$

4.2.3 Longitudinal slip standard deviation

The last method aims at minimizing the longitudinal slip standard deviation. Hence, the objective function is now [5]:

$$J = \min_{\mathbf{T}} \sqrt{\sum_{i=1}^{4} \frac{\sigma_{x_i}^2}{4} - \left(\sum_{i=1}^{4} \frac{\sigma_{x_i}}{4}\right)^2}. \tag{4.31}$$

Under the hypothesis of small slip angle each tire's longitudinal force F_{x_i} can be considered as a linear function of the slip σ_{x_i} as in equation (3.17); combining this with (4.25), one gets:

$$\sigma_{x_i} = \frac{T_i}{RC_{\sigma_i}} \tag{4.32}$$

As before, a vector expression of the objective function is needed, so the following vectors and matrices are introduced:

$$\mathbf{T} = \begin{bmatrix} T_1 \\ T_2 \\ T_3 \\ T_4 \end{bmatrix}; \mathbf{w}^T = \begin{bmatrix} 1 \\ 1 \\ 1 \\ 1 \end{bmatrix};$$

$$\mathbf{M} = \begin{bmatrix} \frac{1}{RC_{\sigma_1}} & 0 & 0 & 0 \\ 0 & \frac{1}{RC_{\sigma_2}} & 0 & 0 \\ 0 & 0 & \frac{1}{RC_{\sigma_3}} & 0 \\ 0 & 0 & 0 & \frac{1}{RC_{\sigma_4}} \end{bmatrix}.$$

Rearranging the initial equation using the new variables, the final formulation of the problem is:

$$\min_{\mathbf{T}} \quad J = \left[\frac{1}{4}\mathbf{T}^T\mathbf{M}^T\mathbf{M}\mathbf{T} - \left(\frac{1}{4}\mathbf{w}\mathbf{M}\mathbf{T}\right)^2\right]^{\frac{1}{2}} \tag{4.33}$$

$$\text{s.t.} \quad \mathbf{B}_{TV}\mathbf{T} - \mathbf{c} = 0 \tag{4.34}$$

$$\mathbf{T} - \mathbf{T}_{min} \geq 0 \tag{4.35}$$

$$\mathbf{T}_{max} - \mathbf{T} \geq 0 \tag{4.36}$$

Again, te problem is constrained by the restrictions analyzed in the previous section.

4.3 Gradient method

A brief description of gradient method is presented, since it has been chosen to solve the optimization problem.Gradient method permits to find the optimal solution (if it exists) to a constrained minimum objective function problem; the transient that leads to the solution could at some moment stop fulfilling the required constraints, but the final solution is ensured to be optimal.

Considering the following problem formulation [14, 15]:

$$\min_{\mathbf{x}} \quad J = f(\mathbf{x}) \tag{4.37}$$

$$\text{s.t.} \quad \mathbf{A}\mathbf{x} - \mathbf{b} = 0 \tag{4.38}$$

$$g(\mathbf{x}) \leq 0 \tag{4.39}$$

where $\mathbf{x} \in \mathbb{R}^n$, $f(\mathbf{x}) : \mathbb{R}^n \to \mathbb{R}$ is a strictly convex function, $\mathbf{A} \in \mathbb{R}^{m\times n}$, $\mathbf{b} \in \mathbb{R}^m$ and $g(\mathbf{x}) = (g_i(\mathbf{x})), i = 1, \ldots, p : \mathbb{R}^n \to \mathbb{R}$ are convex and $\boldsymbol{C}^2$-class functions, the solution proposed by gradient method is:

$$\begin{cases} \boldsymbol{\tau}\dot{\mathbf{x}} = -\nabla f(\mathbf{x}) - \mathbf{A}^T\boldsymbol{\lambda} - \sum_{i=1}^{p} \boldsymbol{\mu}_i \nabla g_i(\mathbf{x}) \\ \boldsymbol{\kappa}\dot{\boldsymbol{\lambda}} = \mathbf{A}\mathbf{x} - \mathbf{b} \\ \boldsymbol{\gamma}_i\boldsymbol{\mu}_i = [g_i(\mathbf{x})]^+_{\mu_i} \end{cases} \tag{4.40}$$

being $\boldsymbol{\tau} \in \mathbb{R}^{n\times n}$ positive semidefinite, $\boldsymbol{\lambda} \in \mathbb{R}^m$, $\boldsymbol{\gamma}_i > 0$ for $i = 1, \ldots, p$, and

$$[g_i(\mathbf{x})]^+_{\mu_i} = \begin{cases} g_i(\mathbf{x}) & \boldsymbol{\mu}_i > 0 \\ 0 & \boldsymbol{\mu}_i = 0 \end{cases} \tag{4.41}$$

The parameters $\boldsymbol{\tau}$, $\boldsymbol{\kappa}$ and $\boldsymbol{\gamma}_i$ can be modified to tune the resolution process, producing significant changes in the shape of the solution curve (oscillations, maximum reached value, etc.) that could result useful, for example, to reduce the computational time. If a solution exists, gradient method algorithm will find the optimal one; nevertheless, it is possible that during the transient phase the solution does not meet the constraints for a short period of time. This must be taken into account when the method is be used to produce an on-line torque allocation: the dynamics of the torque distribution will have to be much faster than the vehicle dynamics, in order to ensure the use of the stable optimal value.

4.4 Torque allocation via gradient method

An optimal torque allocator is proposed, using gradient method to solve the constrained optimization problem. For the sake of simplicity, the longitudinal slip power loss cost function is chosen for the example, since it is the only one in quadratic form.

Introducing (4.20), (4.21), (4.22) and (4.23) in the system described in (4.40) yields:

$$\begin{cases} \boldsymbol{\tau}\dot{\mathbf{T}} = -2\mathbf{D}\mathbf{T} - \mathbf{B}_{TV}^T\boldsymbol{\lambda} + \boldsymbol{\mu}_1 - \boldsymbol{\mu}_2 \\ \boldsymbol{\kappa}\dot{\boldsymbol{\lambda}} = \mathbf{B}_{TV}\mathbf{T} - \mathbf{c} \\ \boldsymbol{\gamma}_1\boldsymbol{\mu}_1 = [\mathbf{T}_{min} - \mathbf{T}]^+_{\mu_1} \\ \boldsymbol{\gamma}_2\boldsymbol{\mu}_2 = [\mathbf{T} - \mathbf{T}_{max}]^+_{\mu_2} \end{cases} \tag{4.42}$$

The system was implemented in Simulink and tested before being introduced in the full model. Simulations showed that a stable solution is found, however the transient time is quite long and oscillation are present. The performance can be enhanced by studying the stability of the system and by properly changing the values of the tuning parameters.

First of all, the linearized system including the cost function and the equality constraint is computed. At this point the tuning parameters are neglected and will be reintroduced later. Under the hypothesis of very small steering angle δ the following simplifications are adopted: $\sin\delta \approx 0$, $\cos\delta \approx 1$. The resulting system is:

$$\dot{\mathbf{z}} = \mathbf{H}\mathbf{z} + h(\mathbf{z}) \tag{4.43}$$

where

$$\mathbf{z} = \begin{bmatrix} \mathbf{T} \\ \boldsymbol{\lambda} \end{bmatrix}; \tag{4.44}$$

$$\mathbf{H} = \begin{bmatrix} -\frac{2V_{w,1}}{R^2 C_{\sigma_1}} & 0 & 0 & 0 & -\frac{1}{R} & \frac{c_f}{2} \\ 0 & -\frac{2V_{w,2}}{R^2 C_{\sigma_2}} & 0 & 0 & -\frac{1}{R} & -\frac{c_f}{2} \\ 0 & 0 & -\frac{2V_{w,3}}{R^2 C_{\sigma_3}} & 0 & -\frac{1}{R} & \frac{c_r}{2} \\ 0 & 0 & 0 & -\frac{2V_{w,4}}{R^2 C_{\sigma_4}} & -\frac{1}{R} & -\frac{c_f}{2} \\ \frac{1}{R} & \frac{1}{R} & \frac{1}{R} & \frac{1}{R} & 0 & 0 \\ -\frac{c_f}{2} & \frac{c_f}{2} & -\frac{c_r}{2} & \frac{c_f}{2} & 0 & 0 \end{bmatrix}, \tag{4.45}$$

and $h(\mathbf{z})$ is the non-linear not tuned part.

By looking at the eigenvalues of $\mathbf{H}$ one can see that the system is stable, since all of them have negative real part; furthermore, there are two pairs of complex conjugate poles. The next step aims at reducing the oscillation by removing the imaginary part of the poles and at shortening the transient part by properly positioning the poles in the left half-plane.
This can be made in MATLAB with the command *place*, with some adjustments due to the syntax. Moving the poles towards left in the negative real half-plane reduces the transient time needed to converge to the optimal solution, thus ensures that the torque allocation can be made without discretizing the process.

Chapter 5

Control

5.1 Control structure

The main idea is to divide the control process into different levels, in order to treat properly the various subsystems that compose the vehicle and focus on the ones of interest. At the end of the control structure there is the vehicle model, which receives the input from the low-level controller and produces as output the correspondent behavior of the car measured in the variables r and β. These are the variables in the feedback loop that combined with the steering input o f the driver generate the yaw rate reference, at the top of the control structure. The general structure is shown is Fig. 5.1.
The high-level controller is responsible of calculating the desired yaw moment needed to track the reference, a fundamental step for good results. Desired characteristics of this controller are: tracking with low transient time and reduced oscillations, robustness and smoothness of the control law.
The latter block is the one regarding the torque allocation: the desired yaw moment and longitudinal drive/brake force feed the optimizer, which generates the values of the torques that the four motors must supply to the wheels. The dynamics of this process has to be much faster than the vehicle dynamics, if an on-line allocation without discretization is wanted; obviously stability and robustness are necessary too.
The already mentioned controllers are the key parts of the entire control process, the ones this project actually focuses on. Anyway, there are some more control blocks required to model the entire vehicle. Between the torque allocation and the vehicle model, the

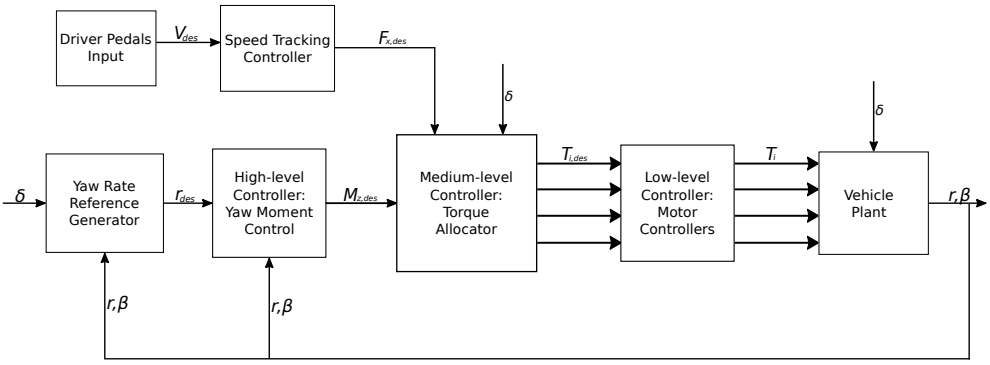

Figure 5.1: General control structure

low-level controller transmits the generated desired torques as input signal to the motors, as to produce the real torques and feed the model with them. This step is important because sometimes the motors cannot follow exactly the shape of the desired torque curve, because it is too irregular or changes too fast, so if the model is fed with the real torques an error will arise. In any case, the physics of the electric motors imply a transient time to actuate and produce a desired torque, which added to the time needed to transmit the signal will result in a delay of the vehicle behavior with respect to the ideal on-line model. Another fundamental block is the one that receives the inputs from the driver through the pedals and calculates the needed longitudinal drive/brake force. In this project a constant speed is supposed to be desired, so the overall F_x is calculated applying the inverse dynamics of the longitudinal model presented in Section 3.1.1. With this simplification, the translation of the pedal pressures into a desired speed or force is neglected, since the constant desired speed is taken as a known parameter.

5.2 High-level controller

In this chapter two types of controllers for the direct yaw control (DYC) will be described and implemented. The DYC is the high-level controller, which receives the desired yaw rate and generates the yaw moment needed to track the reference. The controller has to be fast and robust, and the generated yaw moment must have a value that could be actually produced by a proper torque allocation.

As presented in Section (3.3.1), the yaw rate reference is calculated from the steering angle input and the vehicle speed as in (3.3.1).

The controllers will be tested through simulations in Simulink, using different steering wheel's input curves that represent some of the typical test maneuvers. These include a step, a ramp, a smooth J-turn, an approximated single lane change and a double lane change.

The two proposed solutions consist in a combined PID and sliding-mode control, and a model reference adaptive control (MRAC). For each of them the advantages and drawbacks will be analyzed, with the objective of finding a feasible and adequate solution integrated with the rest of the vehicle model.

5.3 Combined PID and sliding-mode control

The proposed control includes a standard PID block and a sliding-mode block which work in parallel to track the reference. The idea is that through a proper tuning of the control parameters, the two controllers could cooperate and compensate each other's drawbacks and deficiencies. Obviously the sliding-mode is the predominant one and strictly necessary to achieve satisfying results, since it is easily proved that the PID itself is not capable of tracking the reference. A brief analysis of the two control laws formulation is now presented.

The proportional integrative and derivative part of the control scheme is in its standard form: the input signal is the yaw rate tracking error defined as $\tilde{r} = r_{ref} - r$, and the produced control law $M_{z,des,PID}$ is computed as:

$$M_{z,des,PID} = \left(K_P + \frac{1}{s} K_I + s K_D \right) \tilde{r} \tag{5.1}$$

where K_P, K_I and K_D are, respectively, the proportional, integrative and derivative gain. As said, this controller by itself cannot track the reference properly, hence the need to combine it with another one.

Sliding-mode control (SMC) usually ensures good tracking, fast response and high robustness, despite the presence of chattering in the control law due to the commuta-

tion term in its formulation. The main idea is that the control law "slides" on a desired switching surface, switching is produced by the sign function of the sliding surface, so the presence of non-linearities and chattering. A sufficiently high gain usually ensures controllability, good performances and robustness.

In this case, the sliding surface is chosen as:

$$\sigma = r - r_{ref}, \tag{5.2}$$

and the control law is calculated as:

$$M_{z,des,SMC} = -\text{sgn}(\sigma) J_z K_{SMC}, \tag{5.3}$$

being K_{SMC} the static gain applied. The asymptotic stability of $\sigma = 0$ is demanded through the Lyapunov theorem, so the inequality $\dot{V} < 0$ has to be verified. A Lyapunov function is defined as:

$$V = \frac{1}{2}\sigma^2, \tag{5.4}$$

so deriving and rearranging the terms using (4.4) and (5.3) one gets:

$$\dot{V} = \sigma\dot{\sigma} = \sigma\dot{r} = \sigma\left(\frac{1}{J_z}\right)\left[M_{z,unc}(r,\beta,\delta) - \text{sgn}(\sigma) J_z K_{SMC}\right], \tag{5.5}$$

where $M_{z,unc}(r,\beta,\delta) = M_{z,y} + M_{z,SAT} + M_{z,d}$ includes all the uncontrollable terms of the yaw moment (generated by lateral tire forces, self aligning torques and disturbances). Finally, the derivative of the Lyapunov function is negative if

$$K_{SMC} > \left|\frac{M_{z,unc}}{J_z}\right| \tag{5.6}$$

which is the restriction on the controller gain that ensures asymptotic stability [9].

Due to the commutation of the sign function, the SMC usually produces high frequency oscillations both in the control and in the state. These could be attenuated through a low-pass filter, that with a proper cut-off frequency can soften the signal without losing its effectiveness. The gain as well can be adjusted to meet a trade-off between good performance and low amplitude oscillations.

Once the two control laws are generated, they are combined and the result is one of the feed signals of the medium-level controller (the torque allocator):

$$M_{z,des} = M_{z,des,PID} + M_{z,des,SMC} \tag{5.7}$$

5.4 Model reference adaptive control

An alternative solution to the sliding mode control is the model reference adaptive control (MRAC) [16]. Its architecture includes a parameter estimation to face uncertainties of the system, a reference model to follow, and an adaptive algorithm that modifies the control law to make the plant behave as the desired model.
If the parameter estimation and the adaptive algorithm run simultaneously it is called direct MRAC, if they run separately it is called indirect MRAC. In this case an indirect MRAC has been used. This type of controller should ensure robustness against changes in the plant, which could be caused by variations of the vehicle parameters or external factors (road and atmospheric conditions) and represent a realistic scenario for simulations.

The path followed to implement the control scheme is the following: first of all the parameter estimator was built and tested with a state feedback controller, then the reference model and the adaptive algorithm were added and tested, and finally the whole scheme was redesigned with an augmented plant and an integrator to eliminate steady state errors.

5.4.1 Parameter estimation

The objective is to estimate the plant with a linear state space system, which will be later compared with the reference model to generate the adaptive control law. Two approaches are possible: to estimate directly the coefficients of the state space matrices, or to estimate the parameters of the transfer function and, if necessary, calculate the matrices afterwards. They should be equal, but in this particular case the second approach showed better results during simulations despite the presence of an intermediate step.

Starting from the standard state space system in the form

$$\begin{cases} \dot{\mathbf{x}} = \mathbf{A}\mathbf{x} + \mathbf{B}u \\ \mathbf{y} = \mathbf{C}\mathbf{x} + \mathbf{D}u \end{cases} \tag{5.8}$$

with

$$u = -\mathbf{k}_x\mathbf{x} + k_r x_{ref} \tag{5.9}$$

it is possible to calculate the transfer function of every output with the formula

$$\frac{y(s)}{u(s)} = \frac{b_0 s + b_1}{s^2 + a_1 s + a_2} = \mathbf{C}(\mathbf{I}s - \mathbf{A})^{-1}\mathbf{B}. \tag{5.10}$$

In the considered system there are two outputs, r and β, so two transfer functions have to be estimated. Since the control action is the same, they share the same denominator; hence, there are six parameters to estimate, two for the denominator and two for each numerator.

Instead of the torques vector $\mathbf{T}$, the correspondent produced yaw moment $M_{z,x}$ was taken as the action u, which reduces considerably the computational complexity. Two identical estimators were built to estimate both r and β, keeping in mind that the resulting parameters for the denominators have to be equals.

The estimation is carried out as follows, and the procedure is exactly the same for the two variables: for a generic transfer function in the form

$$\frac{y(s)}{u(s)} = \frac{b_1 s + b_0}{s^2 + a_0 s + a_0} \tag{5.11}$$

the parameters vector $\boldsymbol{\theta}$ is defined as

$$\boldsymbol{\theta} = \begin{bmatrix} b_1 \\ b_0 \\ a_1 \\ a_0 \end{bmatrix}$$

and it is estimated as

$$\dot{\hat{\boldsymbol{\theta}}} = -\boldsymbol{\Gamma}(\hat{\boldsymbol{\theta}}^{\boldsymbol{T}}\boldsymbol{\phi} - q)\boldsymbol{\phi}, \tag{5.12}$$

where

$$q = \frac{s^2}{\Lambda(s)} \tag{5.13}$$

$$\boldsymbol{\phi} = \begin{bmatrix} \frac{su}{\Lambda(s)} \\ \frac{u}{\Lambda(s)} \\ -\frac{sy}{\Lambda(s)} \\ -\frac{y}{\Lambda(s)} \end{bmatrix} \tag{5.14}$$

$$\boldsymbol{\Gamma} = \begin{bmatrix} \gamma_1 & 0 & 0 & 0 \\ 0 & \gamma_2 & 0 & 0 \\ 0 & 0 & \gamma_3 & 0 \\ 0 & 0 & 0 & \gamma_4 \end{bmatrix}. \tag{5.15}$$

$\gamma_1, \ldots, \gamma_4 \geq 0$ are parameters that can be modified to tune the speed of the process, while $\Lambda(s)$ is a second order stable filter in the form

$$\Lambda(s) = s^2 + \lambda_1 s + \lambda_0 \tag{5.16}$$

where $\lambda_0, \lambda_1 > 0$ can be arbitrarily set to obtain the desired dynamics of the filter. The estimation of the state variable is

$$\hat{q} = \hat{\boldsymbol{\theta}}^{\boldsymbol{T}}\boldsymbol{\phi}. \tag{5.17}$$

This variable can be compared with the plant output (graphically or analytically) to verify the correctness of the estimation.

There are two factors that affect significantly the estimation: the input signal ϕ has to be persistently exciting (PE), and the initial conditions of the estimation should be sufficiently close to the final result.
If the input is not PE, for example a constant input, the estimation could slightly increase the steady state error, which implies the impossibility of tracking the reference with good performance. Anyway, it is quite uncommon to have a not-PE input, that should mean a cornering maneuver with a steer angle kept for constant for a long time, so, as simulations

will show, results are not affected by this problem.
As regards the initial conditions, if they are too far from the actual system, the estimator could be either unable of finding a solution or too slow to reach it in an acceptable time. This can be avoided if a rough estimation of the system is known (as in the case of a vehicle, many parameters are known or in a known range of values): this nominal system will be set as starting point of the estimation. Specifically, the linearized system with constant parameters was taken as initial condition of the estimation.
Another difficult scenario is the case of harmonic input: for a second-order system there are infinite solutions that behave in the same way at two frequencies; hence, it is possible that a wrong estimation produces correct results at determined frequencies. This mistake can be prevented again by setting the initial conditions sufficiently close to the expected result. Furthermore, a long sinusoidal input is an unrealistic situation.

Once the parameters of the transfer functions are estimated, the next step is to write the matrices $\hat{\mathbf{A}}$ and $\hat{\mathbf{B}}$ of the estimated plant with equation (5.10) and feed them into the adaptive control algorithm.

5.4.2 Adaptive algorithm

First of all the plant is augmented to reject steady state errors with an integrator. The result is a third-order system, so the reference model must have the same dimension. The final formulation is:

$$\begin{cases} \dot{\mathbf{x}} = \mathbf{A}\mathbf{x} + \mathbf{B}u \\ y = \mathbf{C}\mathbf{x} \\ u = -\mathbf{k}\mathbf{x} - k_z z \\ \dot{z} = y_{ref} - y \end{cases} \tag{5.18}$$

Rearranging the terms the system can be written in the form

$$\dot{\mathbf{x}}_A = \mathbf{A}_A \mathbf{x}_A + \mathbf{b}_A y_{ref} \tag{5.19}$$

i.e.:

$$\begin{bmatrix} \dot{\mathbf{x}} \\ \dot{z} \end{bmatrix} = \begin{bmatrix} \mathbf{A} - \mathbf{B}\mathbf{k} & -\mathbf{B}k_z \\ -\mathbf{C} & 0 \end{bmatrix} \begin{bmatrix} \mathbf{x} \\ z \end{bmatrix} + \begin{bmatrix} 0 \\ 0 \\ 1 \end{bmatrix} y_{ref} \tag{5.20}$$

The system is now of the third order, but the actual dynamics of the plant are still of second-order. Thus, the reference model must be of the third order to match with the augmented plant but must behave like a second-order system as the physical plant is. This can be achieved by building the reference model matrix following a pole placement procedure.

The final pole set is a pair of complex conjugate poles (chosen to achieve desired performances in terms of settling time and overshoot) and a stable real pole at least ten times faster than the others. With this choice the dynamics of the reference model is completely dominated by the conjugate pair of poles, while the effects of the third pole can be neglected.

Once the poles are known, the reference matrix $\mathbf{A}_m$ is calculated in this way:

$$det(\mathbf{A}_m - \lambda\mathbf{I}) = (\lambda - p_1)(\lambda - p_2)(\lambda - p_3) \tag{5.21}$$

where p_1, p_2, p_3 are the desired poles and $\mathbf{A}_m$ is a 3×3 matrix in the form

$$\mathbf{A}_m = \begin{bmatrix} \mathbf{A}_{m_{1,1}} & \mathbf{A}_{m_{1,2}} \\ -\mathbf{C} & 0 \end{bmatrix} \tag{5.22}$$

The final step is the generation and update of the control action. The controlled system of eq. (5.20) is forced to be equal to the reference model; it must be $\hat{\mathbf{A}} = \mathbf{A}_m$, hence

$$\hat{\mathbf{A}} - \hat{\mathbf{B}}\mathbf{k} = \mathbf{A}_{m_{1,2}} \tag{5.23}$$

$$-\hat{\mathbf{B}}k_z = \mathbf{A}_{m_{1,2}} \tag{5.24}$$

and finally

$$\mathbf{k} = \hat{\mathbf{B}}^{-1}(\hat{\mathbf{A}} - \mathbf{A}_{m_{1,2}}) \tag{5.25}$$

$$k_z = -\hat{\mathbf{B}}^{-1}\mathbf{A}_{m_{1,2}} \tag{5.26}$$

With a proper pole placement, this solution enhances the results previously obtained with the SMC, both in tracking and in the shape of the torque curve, which is a core issue in terms of feasibility. Furthermore, with MRAC is possible to control the system even if there are some unknown or changing parameters.

Chapter 6

Simulations and analysis of the results

In this chapter are shown the simulations and the results of the work presented in the previous parts. All calculations were carried out with MATLAB software, while simulations were implemented in the integrated software Simulink. All simulations are approximated reproductions of real situations, with some simplifications and under certain hypothesis. More accurate simulations could be carried out with more specific softwares, this will be more deeply debated in the next chapter.
The hypothesis made are the following: the vehicle is running at constant and known speed, all the involved vehicle parameters are known or measurable, the time spent by the control signal to reach the motors and the consequent delay are neglected.

First of all simulations were carried out to validate the vehicle model, subsequently the torque vectoring operated through gradient method was tested and validated, finally the two types of control were introduced, tuned, tested and enhanced when possible. One of the most important issues was the compatibility between the controller and gradient method, in terms of possibility to work one beneath the other in real-time without the necessity of discretizing the process to permit off-line calculations.

6.1 Input signals

The main input signals of the simulations are the total longitudinal force and the steer angle. Since the speed is assumed constant, the total longitudinal force is calculated with inverse longitudinal dynamic as described in section 3.1.1 and it is represented as a constant scalar. On the contrary, the steer angle plays a fundamental role in all the parts of the system: in the plant it is necessary to calculate the lateral forces and self aligning moments, it is an indispensable input to the torque vectoring algorithm and it is converted into the desired yaw rate with equation (3.29). This last function is the one that permits to carry out simulations close to real scenarios: every steer angle input curve represents the reproduction of a specific maneuver, generally approximated and steepened taking account of the worst possible situation.
The input steer angle is always expressed in rad and it is the angle at the tires. To find reasonable values, a steer ratio (steering wheel angle/steer angle at the tire) of 15:1 was supposed. For example when the steering wheel is at 90deg, the front tires are turned of $\frac{90}{15} = 6$deg that correspond to a value of δ of 1.05rad. All simulations were carried out with a constant speed of 60km/h. In detail, these are the maneuver that were used in simulations:

- **Step**: this is the most unrealistic case, due to its nonlinear and steep shape, but it helps considerably to understand the dynamics and behavior of a particular controller. With the step response, one can easily study the control performances in terms of settling time and overshooting, identifying at first sight any oscillations or unstable zones.
  Physically speaking, it is an extreme approximation of a steep J-turn with the steering wheel reaching very quickly 90deg and keeping it constant for a long time.

- **Ramp** (not always used): like the previous case, this is an approximation of the J-turn maneuver, a bit "softer" than the step but still far from the real case, due to the presence of discontinuous changes of slope. The final value still corresponds to a 90deg position of the steering wheel, but now it takes 0.5s to reach it.

- **J-turn**: an arctan function was used to reproduce the scenario of a realistic J-turn; with this expedient there are no more discontinuities and the shape of the curve is more gentle. To make the vehicle run perfectly on the desired trajectory, high

precision tracking is searched both in transient and steady state phases.
The final value is again 90deg at the steering wheel and it takes around 2.5s to reach that position.

- **Single lane change**: it is one of the most common maneuver when testing a vehicle, mostly used in its ISO standard version for simulations on real vehicles or with specific softwares. It is so used because includes a large variety of real maneuvers, like a change of line driving on a highway, an overtake, or a sudden move to avoid an obstacle.
  In this project a simplified version was used, outlined as single sine pulsation with steering angle set to zero before and after the maneuver. The amplitude was set to 0.05rad, corresponding to 45deg at the steering wheel, and the period of the wave is $\frac{4}{3}\pi$s.

- **Double lane change**: it is the previous maneuver followed by another sine pulsation, with same amplitude and frequency but with opposite sign (i.e. direction) with respect to the first one, carried out to go back to the initial line. Between the two movements the steer angle is maintained at zero for a short time (less than 1s).

Fig. 6.1 shows the shape of the used curves, while Fig. 6.2 shows how the ISO double lane change maneuver is made in experimental tests.

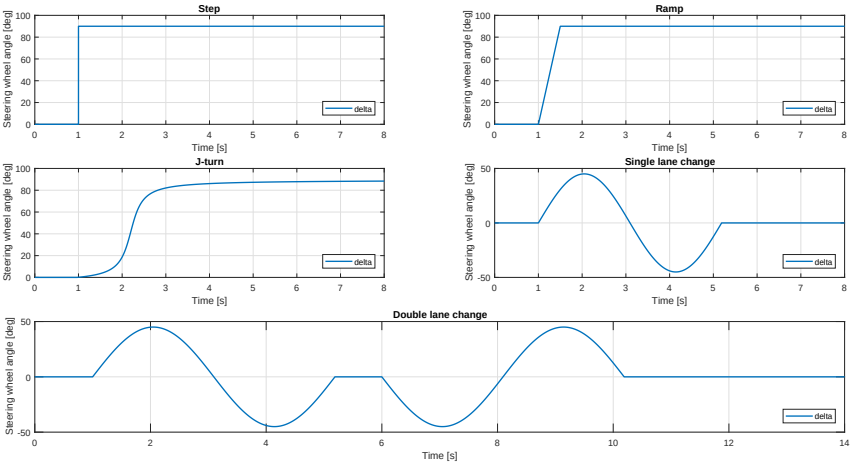

Figure 6.1: Input curves used during simulations

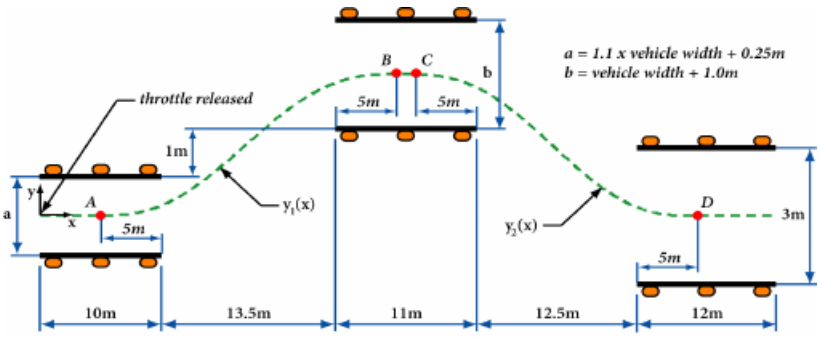

Figure 6.2: ISO double lane change test [17]

6.2 Validation of the torque allocation via gradient method

The torque vectoring block is, together with the control strategy, the core of the project. Before introducing it into the complete model, it was necessary to test it and validate its correctness. This was made through different simulations in open loop, with the block disconnected from the rest of the scheme (controller, plant) and only fed with the needed inputs. The constant parameters were set to the same values of the following complete simulations, the input signals for δ were the ones described in section 6.1. Only the shape of $M_{z,des}$ was unknown, due to the absence of the controller, so different types of curves were used to see how the system would have reacted, often with values close to the limit of existing solution to push the system as much as possible. The longitudinal total drive force is constant, and as initial condition for the torques was taken the case of a basic 4×4 allocation, so any tire is given the same value.

In the subsections below the three cost functions are tested and a first idea of the difference between them is outlined before putting them into the complete model.

6.2.1 Longitudinal slip power loss

Following the order of the previous chapter, the first solution tested was the torque allocation with the longitudinal power slip loss as cost function. images. The first test was made with constant null values for the steer angle and the desired yaw moment, and a total drive force calculated to maintain a certain constant speed: this means that the vehicle is running straight at constant speed.

Fig. 6.3 shows the result of the torque allocation in the described scenario: all wheels receive a positive torque and there is perfect balance between the right and the left side of the vehicle. One can also see that the total force is not split equally between the four motors, but the front wheels receive a bigger value. This is a consequence of the cost function adopted: for the front tires the slip stiffness C_{σ_x} is bigger than for the rear tires, so it is reasonable to allocate on the front side higher torques to minimize the cost function.
With this simple test, one gets to know that with this cost function the distribution of

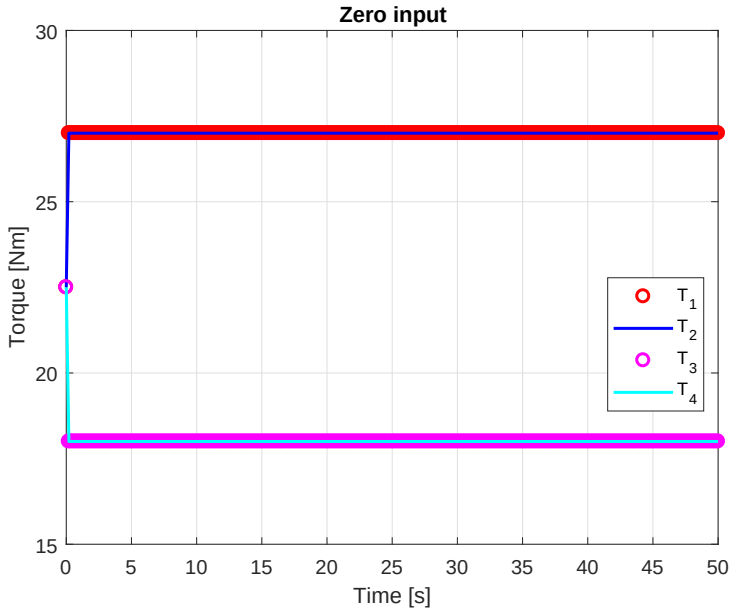

Figure 6.3: Torque distribution of test with zero input and longitudinal slip power loss based TV

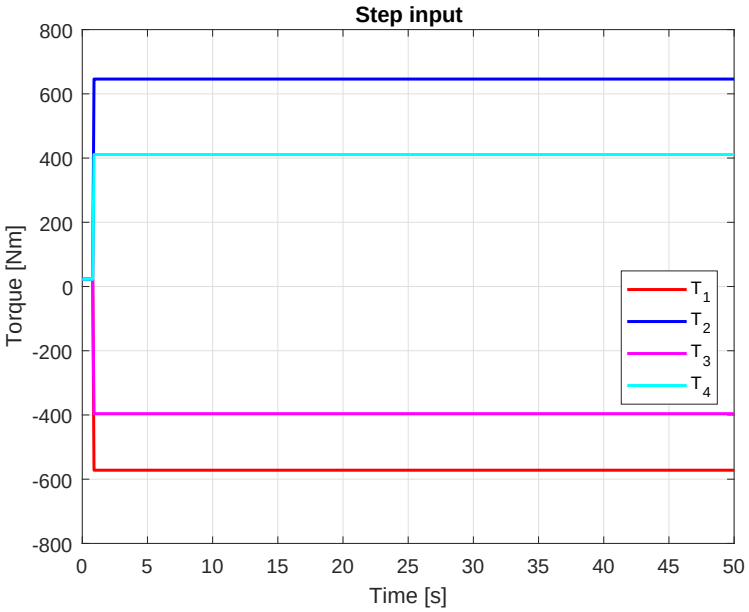

Figure 6.4: Torque distribution of test with step input and longitudinal slip power loss based TV

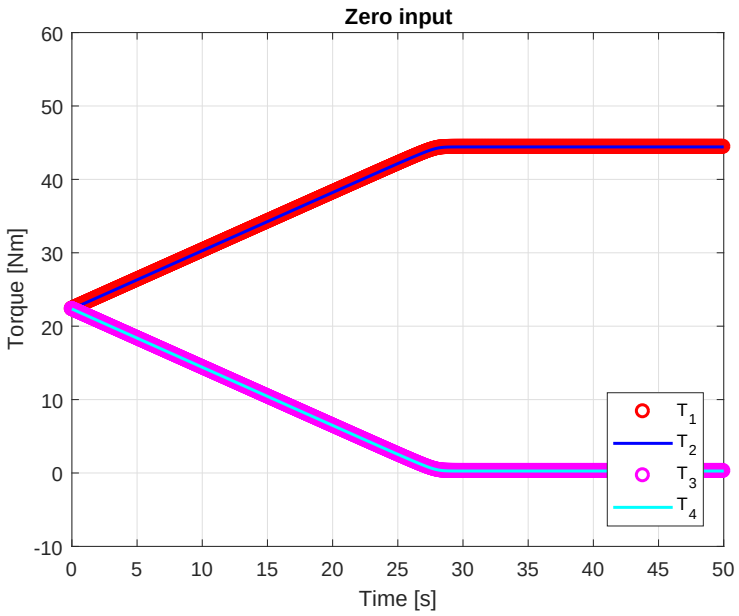

Figure 6.5: Torque distribution of test with zero input and total tire force coefficient based TV

the torque will always tend to be unbalanced towards the front part of the car.

Fig. 6.4 shows results of the test with step inputs for δ and $M_{z,des}$: one can see that the wheels on the outer side are given positive torques, with a higher value to the front one, while both inner wheels receive negative (brake) torques. Since the vehicle is turning left, the result is the one expected, with all the wheels giving a positive contribution to the anti-clockwise yaw moment.
The system is obviously wanted to be stable and fast: in this case, after a proper tuning, it only takes 0.05 s to reach the optimal solution.

6.2.2 Total tire force coefficient

The same simulations were carried out with this objective function. Since the allocator is not linked to any plant, it was not possible to feedback the lateral forces, that thus where set at a constant small value to avoid problems of zero-division.

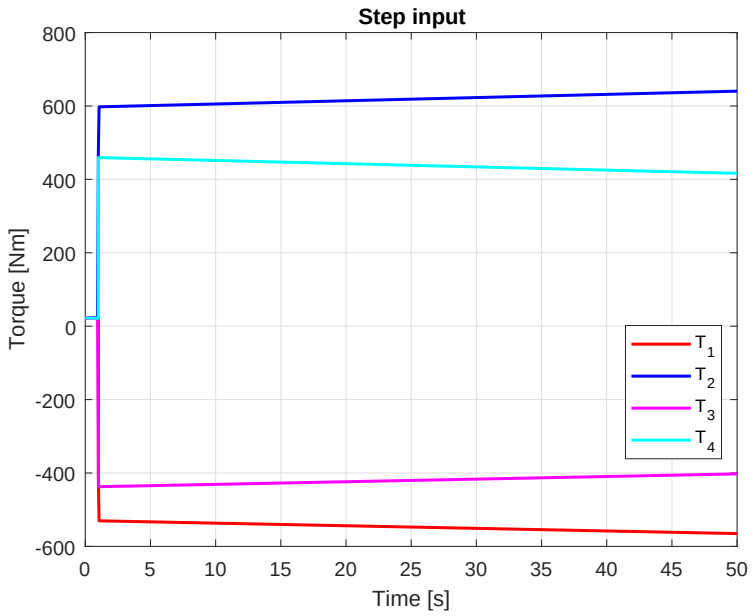

Figure 6.6: Torque distribution of test with step input and total tire force coefficient based TV

Fig. 6.5 and Fig. 6.6 show results of the straight running and step turn simulations, it is immediately clear that with the same tuning parameters the system is much slower than in the previous case but still stable. Increasing the real negative part of the placed poles it is possible to rise the speed until instability starts to appear. Hence, it is necessary to find a compromise between acceptable speed and low risk of instability. The second remarkable difference is that the unbalance between front and rear is higher: the peak values of the front wheels are grater and increasing and they are compensated by lower decreasing values at the rear wheels.
At first glance this solution appears to be less efficient, from speed and balance of the allocation viewpoints.

6.2.3 Longitudinal slip standard deviation

This is the complexest objective function among the chosen, both in terms of implementation and computation. The tests are the same again, with peculiar results: in Fig. 6.7 the test with zero inputs shows a clear unstable behavior. In addition, the poles used in the previous cases were not suitable and had to be shifted to the right in the negative real

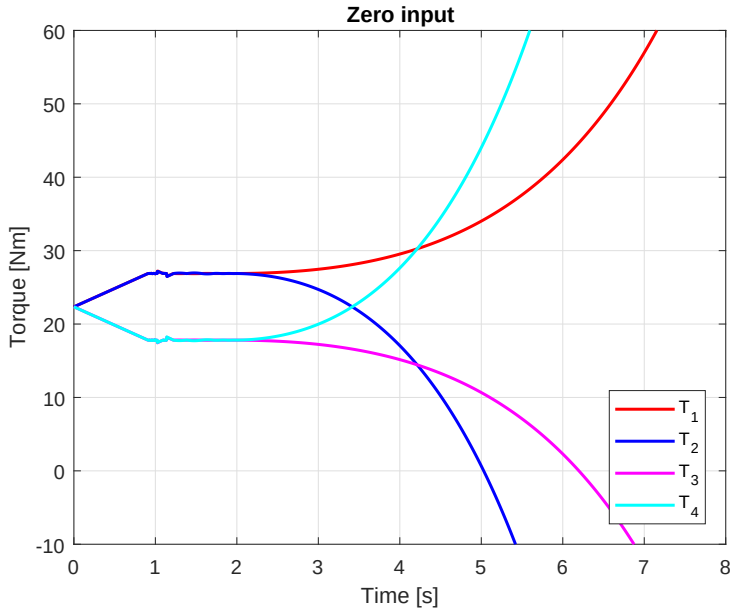

Figure 6.7: Torque distribution of test with zero input and longitudinal slip standard deviation based TV

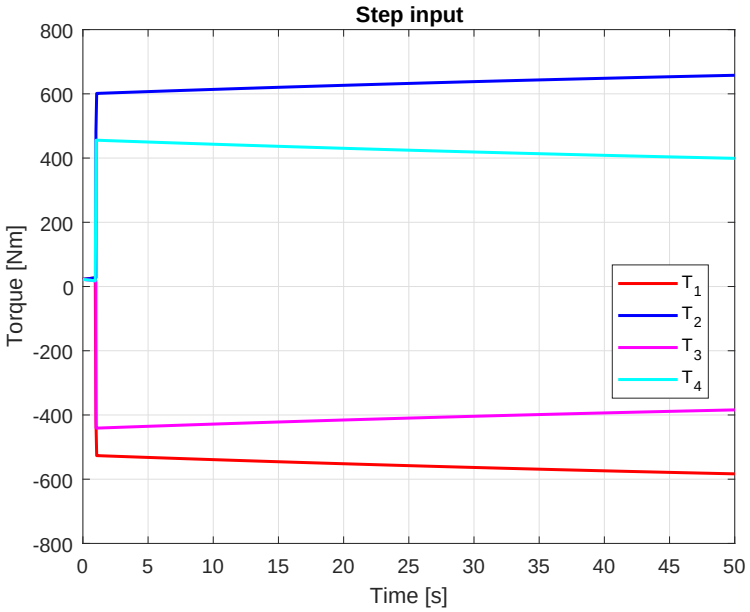

Figure 6.8: Torque distribution of test with step input and longitudinal slip standard deviation based TV

half-plane to complete the simulation.
These drawbacks seem to disappear when the system undergoes non-zero excitations in terms of steer angle and yaw moment, with a behavior close to the previous case: the front-rear unbalance is at first the smallest, but this gap slightly increases with time (Fig. 6.8).

Simulations revealed that when a solution does not exist, the algorithm in Simulink tries to respect the equality constraint even if this implies not to accomplish the other restrictions. Hence, a solution is always found but sometimes it does not respect all the imposed conditions on maximum and minimum torque. Anyway, this problem can be easily solved by adding a saturation function for each torque after the TV block. It is a simple correction but absolutely necessary to make sure that the system is working in physically possible conditions and producing reasonable results.

6.3 Simulations with complete system and longitudinal slip power loss based torque vectoring

In this section, results of simulations of the complete model will be showed and described. After validating the adopted torque allocator, the following step was to connect it to the vehicle model and to the yaw controller. The system is composed as follows: the reference signals for δ are the ones described in Section 6.1, the vehicle plant is in its entire non-linear version, the controller receives the input yaw reference and generates the desired yaw moment to feed the torque allocator, which finally calculates the optimal torque distribution and transmits it to the model. The used cost function is the one the minimizes the longitudinal slip power loss: the choice comes from the fact that it is the simplest and the one that showed the best response during the preliminary assessments. The other objective functions will be analyzed and compared in the next section.

6.3.1 Complete system with SMC

The vehicle is controlled by the combined sliding mode and PID approach described in 5.3. The parameters that could be modified to enhance performances were the three gains

of the PID, K_P, K_D and K_S, and the sliding mode gain K_{SMC}. In addition, a low-pass filter was inserted after the SMC with the objective of eliminating when possible some useless high frequencies oscillations and so to obtain a feasible result in terms of torque curve (if $M_{z,des}$ oscillates, the torque allocator will produce torques oscillating too). Thus, the cut-off frequency of the filter is an extra parameter to adjust.

The results below are the optimal achievable in the described scenario. Even though only the final results are presented, every test underwent an iterative process of tuning to find the best combination of the mentioned parameters.

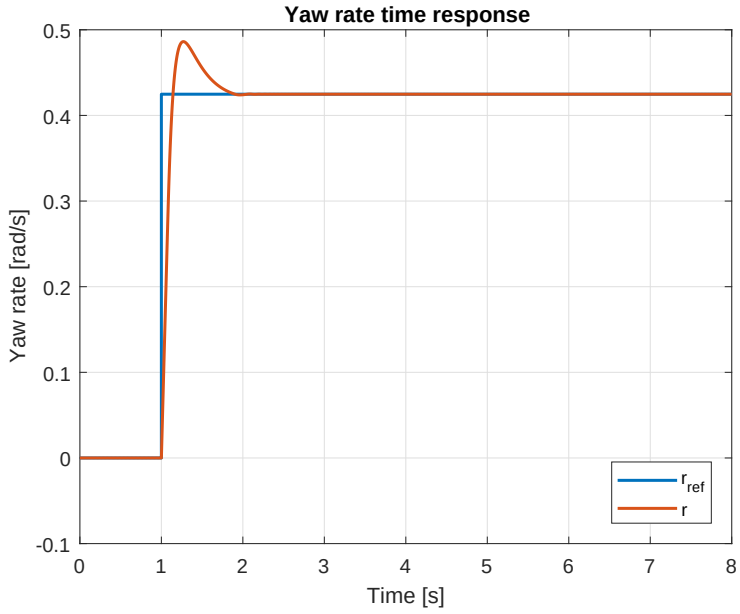

Figure 6.9: Yaw rate time response with step input, SMC and longitudinal slip power loss based TV

The first case analyzed is the response to a step input, which, as said in previous sections, is an extreme and pretty unrealistic case from the physical point of view, but significant to evaluate control performances.
Fig. 6.9 and Fig. 6.10 show respectively the tracking of the yaw rate, and the torque curves at the exit of the TV block. It takes about 1.4s to reach the steady state condition, that coincides with the starting of the oscillations due to the sign function, but after 1s the relative error never exceeds 1.4%. The overshoot peak produces a 14% relative error, that

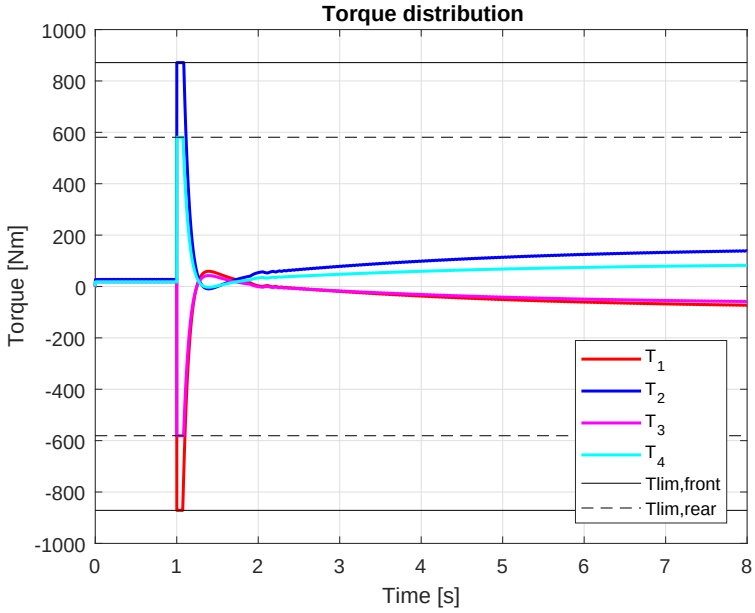

Figure 6.10: Torque allocation with step input, SMC and longitudinal slip power loss based TV

could be reduced decreasing the integrative gain K_I at the expense of a longer settling time. It is important to remember that this situation does not reflect a real maneuver, so the presence of some errors is acceptable until there are no more significant in the following cases.
As regards the torques, one can see that they saturate for 0.07s at the moment of the step, the two right wheels with high positive values, higher for the front wheel, and the left ones with negative values. This is reasonable since an elevate anti-clockwise yaw moment is needed to make the yaw rate follow the reference in a short time. When the system stabilizes, torques fall down of an order of magnitude, but the allocation concept remains the same, with positive values at the outer wheels, slightly braking inner wheels, and higher absolute values at the front axle.

Fig. 6.11 shows the J-turn simulation, now modeled with an arctan function: the reference is almost perfectly tracked, with a small delay ($0.04 \div 0.15$s) between the two significant changes of slope. Furthermore, with the low-pass filter it is possible to eliminate a considerable part of the oscillations in the steady state zone, with vital improvement in terms of torque. In fact, as shown in Fig. 6.12, torque curves have the same shape

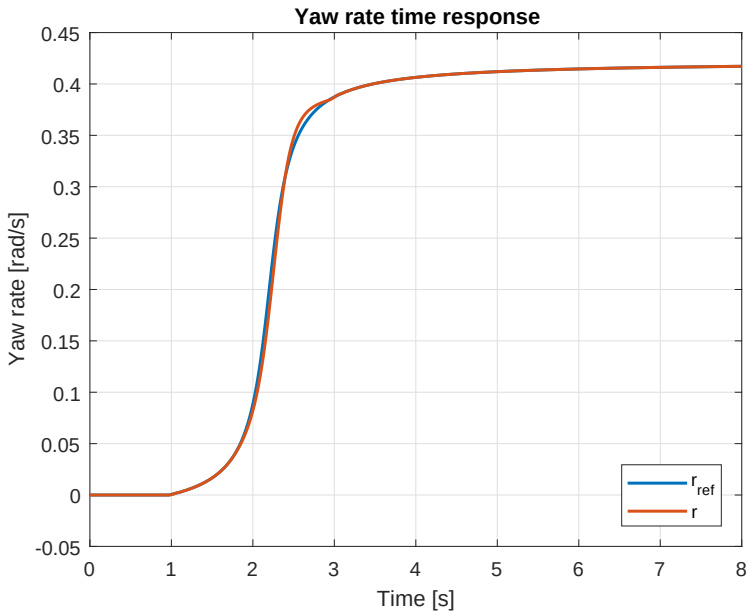

Figure 6.11: Yaw rate time response with J-turn input, SMC and longitudinal slip power loss based TV

as the previous case, but now the peak value is much lower, because of the absence of discontinuities and sharp slope changes. If before the maximum and minimum values were at their limit, now they decreased until 218Nm at the front right wheel and -150Nm at the front left, in correspondence of the steepest zone of the yaw rate curve.

Fig. 6.13 and Fig. 6.14 show respectively details of the yaw rate and torque curves aimed at highlighting the remaining oscillations in the steady state phase: for the yaw rate they have a frequency of 22Hz and a maximum amplitude of $3e^{-4}$rad/s, while for the torque they have the same period with an amplitude of around 3Nm. In both case these oscillations do not have significant effects on the results, since they are at much smaller than the dimensions of the variables they affect.

The last scenarios are the single lane change and double lane change. They are treated together because essentially they are the same maneuver repeated in the opposite direction in the second case. Fig. 6.15 shows that again good tracking is achieved, with a little delay of around 0.06s and overshoot effect especially at the end of the maneuver, with an error of $1.8e^{-2}$rad/s.

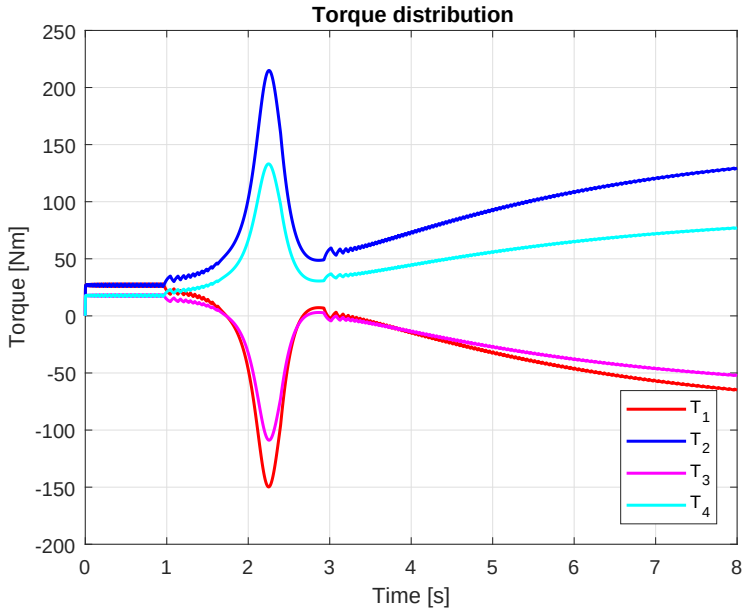

Figure 6.12: Torque allocation with J-turn input, SMC and longitudinal slip power loss based TV

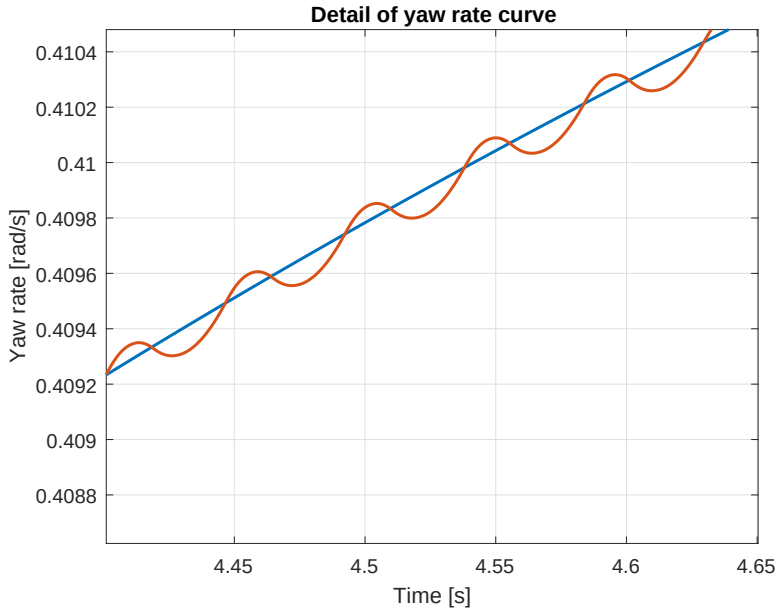

Figure 6.13: Oscillations in yaw rate time response with J-turn input, SMC and longitudinal slip power loss based TV

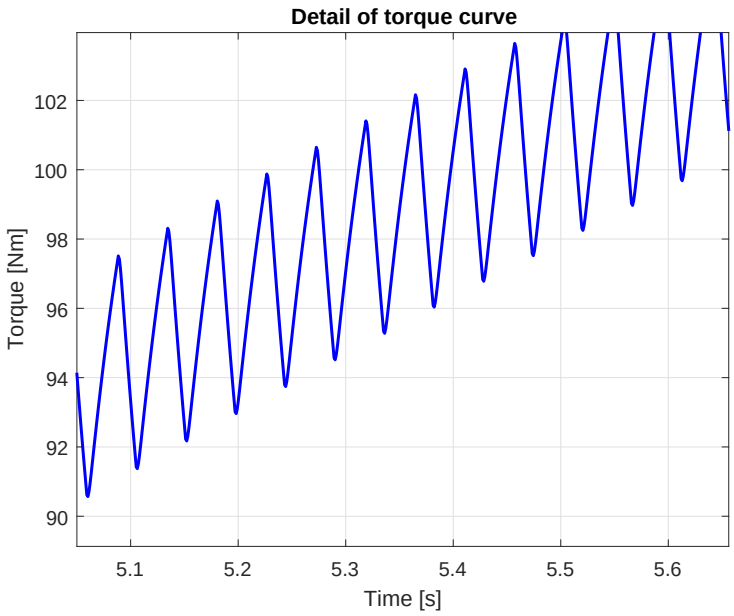

Figure 6.14: Oscillations in torque curve with J-turn input, SMC and longitudinal slip power loss based TV

The graph of the torques in Fig. 6.16 is consistent with the expectations and reasonable. The right and left wheels receive inverse sinusoidal input torques according to this pattern: at the beginning of the maneuver, the steer angle begins to increase with positive sign (with the adopted convention the vehicle is turning left), so the right wheels receive positive torques while the left wheels start braking; successively, right wheels torques decreases and left wheels torques increase as the steer angle approaches its maximum; at this point (around t=2s) there is the crossing between right and left wheel curves, with the second ones becoming greater than the firsts and reaching their maximum (/minimum) for null steer angle; the second part is basically symmetric to the first, with smaller peaks; once the maneuver is over, the unbalance between right and left fades out as the vehicle is now running straight, so $M_{z,des} = 0$ and only the longitudinal drive force has to be generated.
Very small oscillations are present as always in the last part.

As regards the double lane change, results are shown in Fig. 6.17 and Fig. 6.18. The only relevant detail is the fact that in the second line change slightly higher torque peak values are reached. This is the effect of the previous maneuver: in the short break be-

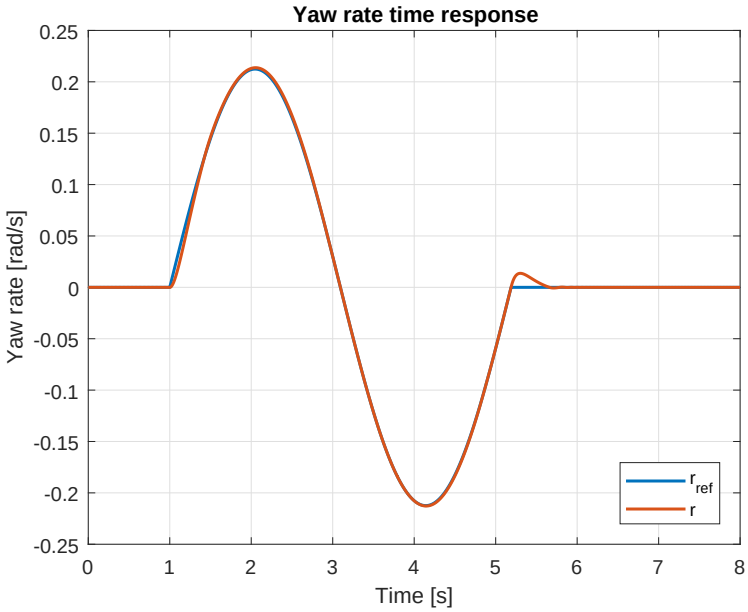

Figure 6.15: Yaw rate time response with single lane change input, SMC and longitudinal slip power loss based TV

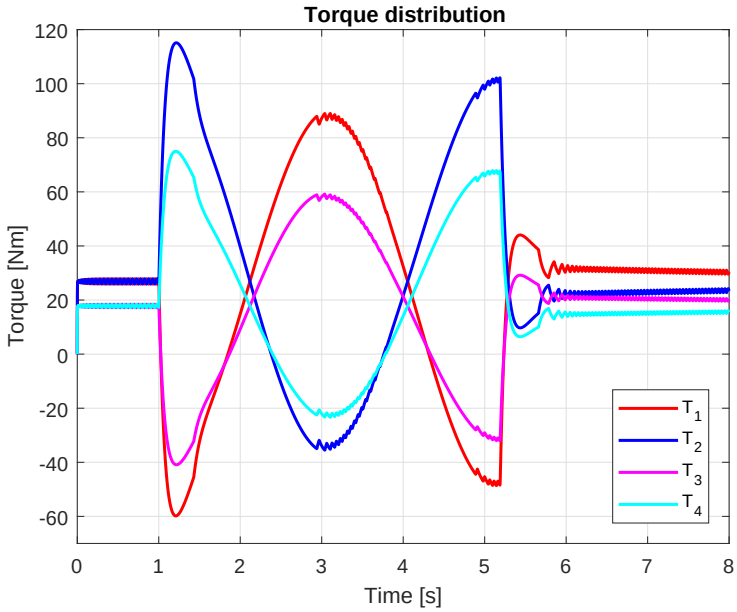

Figure 6.16: Torque allocation with single lane change input, SMC and longitudinal slip power loss based TV

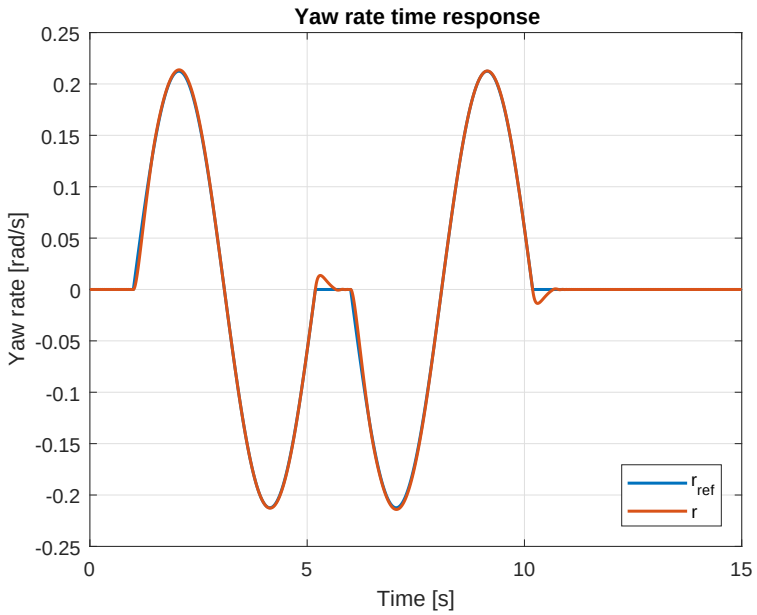

Figure 6.17: Yaw rate time response with double lane change input, SMC and longitudinal slip power loss based TV

tween the two lane changes, a little overshoot is present at the end of the first, and when the second begins both the yaw rate and the torques still have not stabilized. It is not caused by the torque allocator but it is an inevitable consequence of the control law, that could be avoided only extending the time in which the steer angle is kept at zero. Anyway, that increase in the peak value is small and does not imply significant changes or problems.

In conclusion, simulations show two main issues that should be noted: first of all, the SMC and the proposed torque allocator are totally compatible and can work together in continuous time without the need of discretizing the system; this is only possible if the TV dynamics are much faster than the dynamics of the system, which could be achieved thanks to the tuning process designed for the allocation. Second of all, SMC provides satisfying results from any point of view, under the hypothesis of constant known parameters; the only drawback is the presence oscillations, ad direct consequence of the nature of sliding-mode control. Those oscillations can be eliminated by an aggressive low-pass filter, but sometimes this operation could be risky: by cutting a wide range of frequencies, it might result in a degradation of the SMC effectiveness, with consequences that could range from worse performances to the incapability of controlling the system.

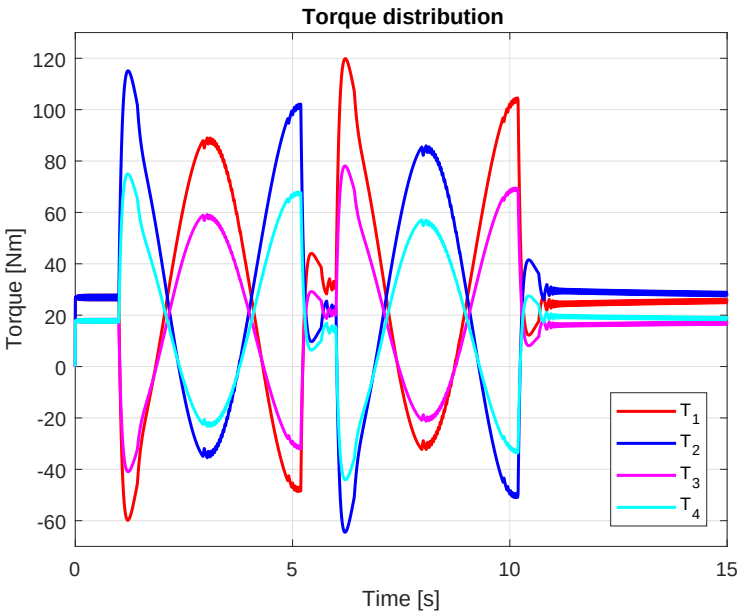

Figure 6.18: Torque allocation with double lane change input, SMC and longitudinal slip power loss based TV

Hence, the optimal solution is a sort of trade-off between high performance with oscillations and lower performance without (or with smaller) oscillations, that should be evaluated for any particular case. For example, if the scenario is a tourism car driven normally, with known parameters and stable external condition, a little imprecision in tracking could be accepted while more comfort is achieved by eliminating all the oscillations. On the contrary, with a sport car or a vehicle in dangerous external conditions (poor road friction, or changing conditions due to rain or snow), the focus is all on having a strong robust control that ensures stability and tracking of the reference in any situation.
Furthermore, there are many ways of making the controller actuate only when necessary by measuring the trend of some variables and introducing a block that decides whether it should be activated or not [8].

6.3.2 Complete system with MRAC

This group of simulations deals with the complete system controlled by MRAC, which is the second control approach treated in the project. The general layout is the same

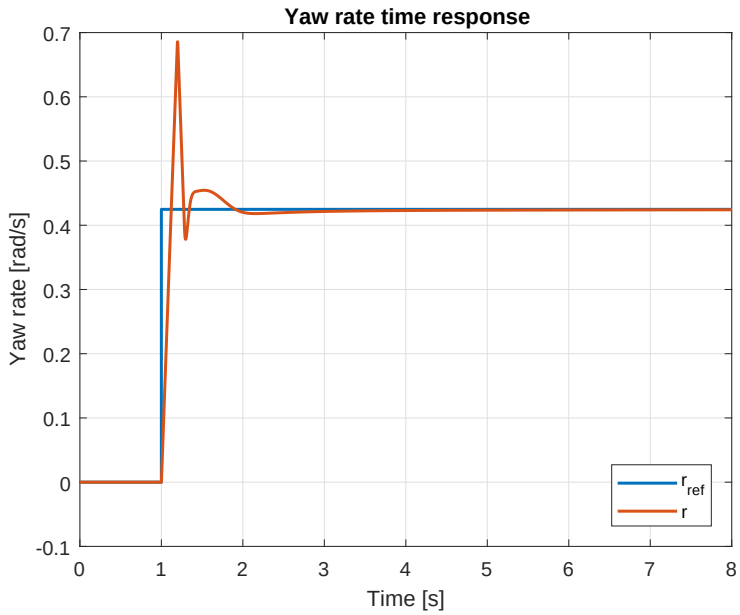

Figure 6.19: Yaw rate time response with step input, MRAC and longitudinal slip power loss based TV

as in the previous section, only the control block changes. In particular, two estimator were introduced for the two states r and β, and then a more complex scheme was built following the theory explained in 5.4. Inputs too are the same as before. The tuning parameters are settling time and overshoot of the reference model, and the variables that control the speed of estimation, explained in Section 5.4.1.

The first analyzed case is the step response. The graph in Fig. 6.19 shows clearly that it is impossible to achieve good tracking of the reference with this system, this control, and this set of restriction. In fact, by looking at Fig. 6.20, one can see that during the transient phase, the torques are all saturated at their maximum or minimum, without acceptable effects on the system: there is 61% overshoot peak and the settling time is absolutely too long.
Anyway, this is a physically irrelevant test, because concretely it represents a tourism vehicle running at 60km/h and suddenly the driver turns the steering wheel of 90deg in an infinitesimal fraction of a second: imagined in this way it is quite obvious that it is hard to control the system with high performances.

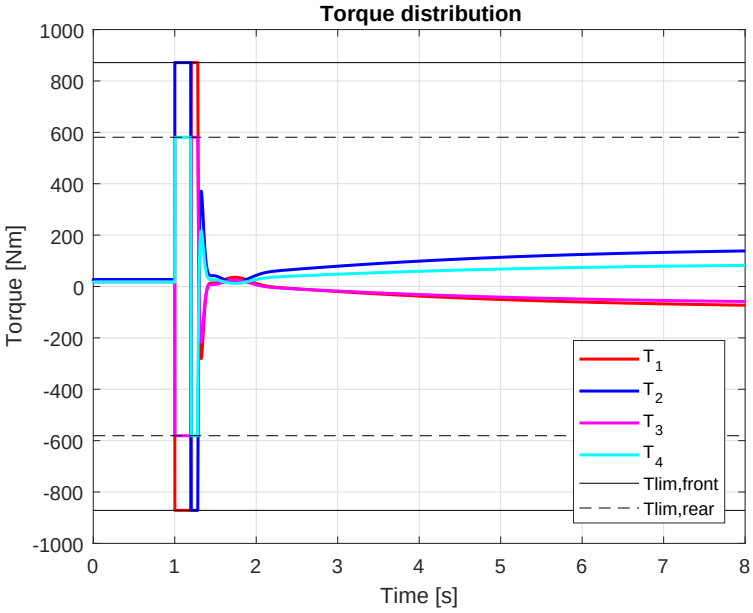

Figure 6.20: Torque allocation with step input, MRAC and longitudinal slip power loss based TV

Results of simulation with the ramp as input are shown in Fig. 6.21 and Fig. 6.22:

the situation improved significantly from the last case, now the reference is tracked satisfyingly, with a 2.6 % error in correspondence of the highest peak. There are no more problems of torque saturation, the extremest values reached are 252Nm and -198Nm, pretty far from the limits. The only remarkable drawback is the presence of small overshoot peaks in correspondence of the two changes of slope of the ramp.

Time response and torque curves of the J-turn simulation are shown in Fig. 6.23 and Fig. 6.24. Tracking of the reference is now almost perfect, with just a delay of less than 0.0015s in the steepest zone and very small oscillations at the beginning of the maneuver and in the final part, when the steer angle is maintained approximately constant. Results on torques are satisfying too, with curves very similar to the analogue case with SMC.

As regards the single lane change, the situation worsens with respect to the previous case, with the apparition of chattering at the end of the maneuver. In the yaw rate curve it is not a compromising issue, as can be seen in Fig 6.25, because the amplitude is small (0.015rad/s at its maximum) and it damps quite fast.

On the contrary, this chattering produces negative effects on the torque allocation: Fig.

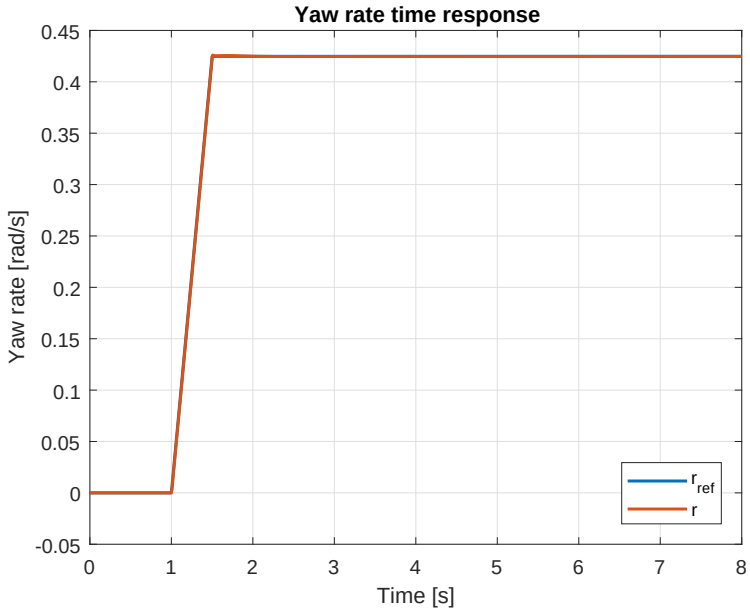

Figure 6.21: Yaw rate time response with ramp input, MRAC and longitudinal slip power loss based TV

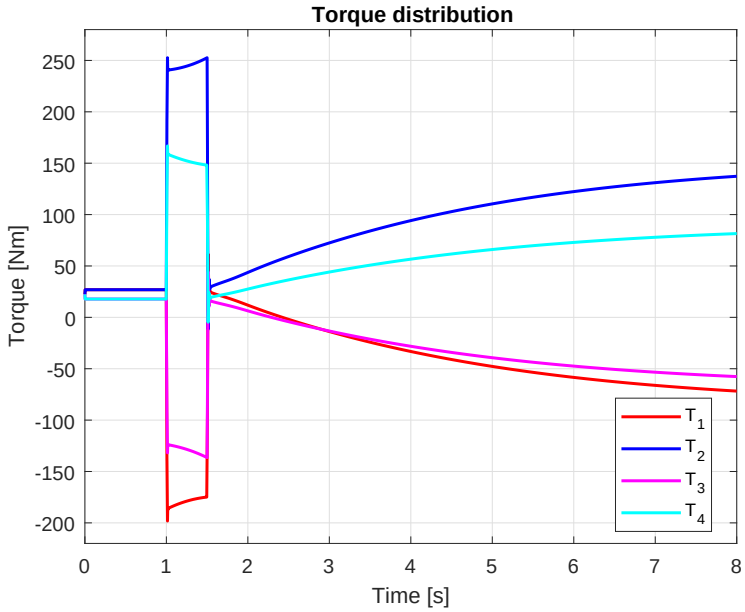

Figure 6.22: Torque allocation with ramp input, MRAC and longitudinal slip power loss based TV

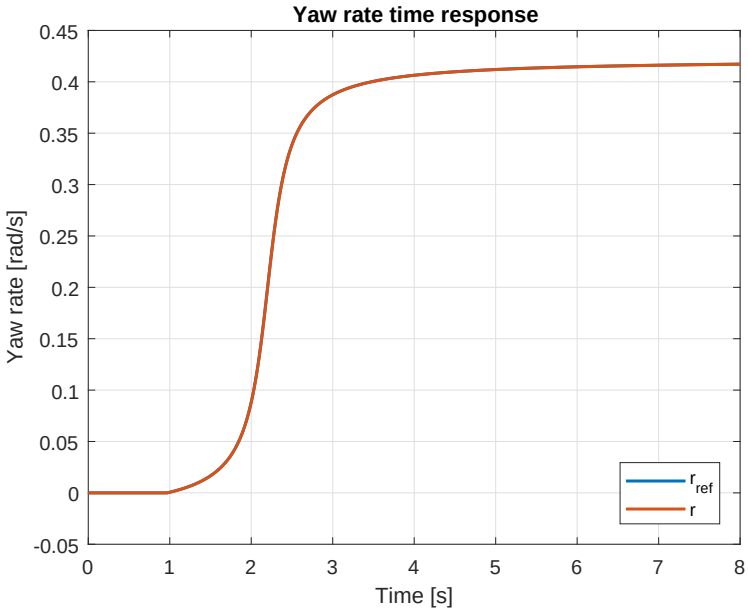

Figure 6.23: Yaw rate time response with J-turn input, MRAC and longitudinal slip power loss based TV

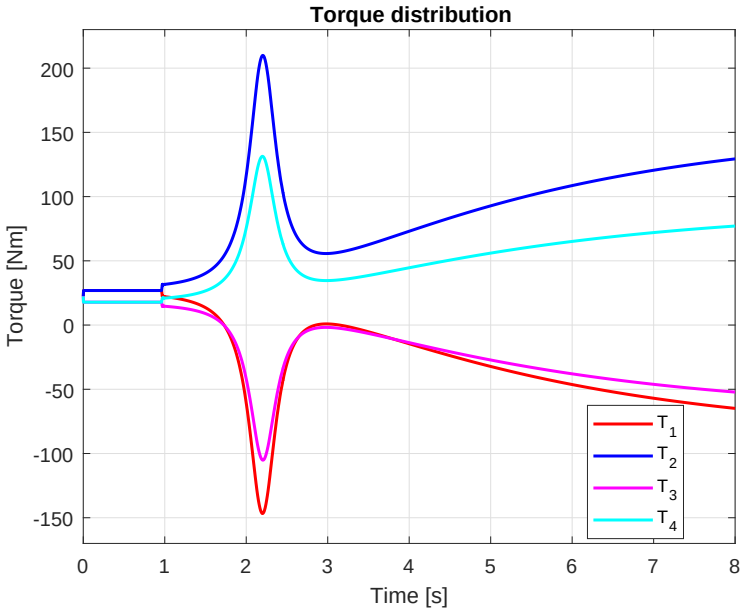

Figure 6.24: Torque allocation with ramp J-turn input, MRAC and longitudinal slip power loss based TV

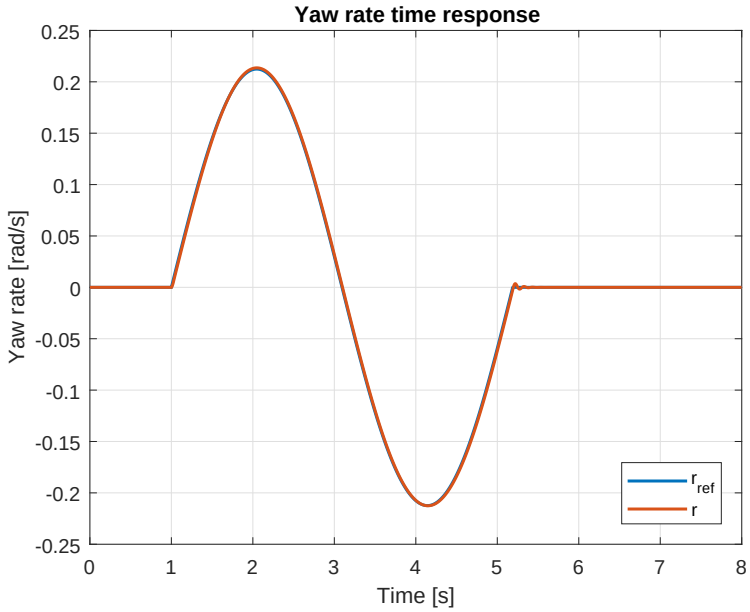

Figure 6.25: Yaw rate time response with single lane change input, MRAC and longitudinal slip power loss based TV

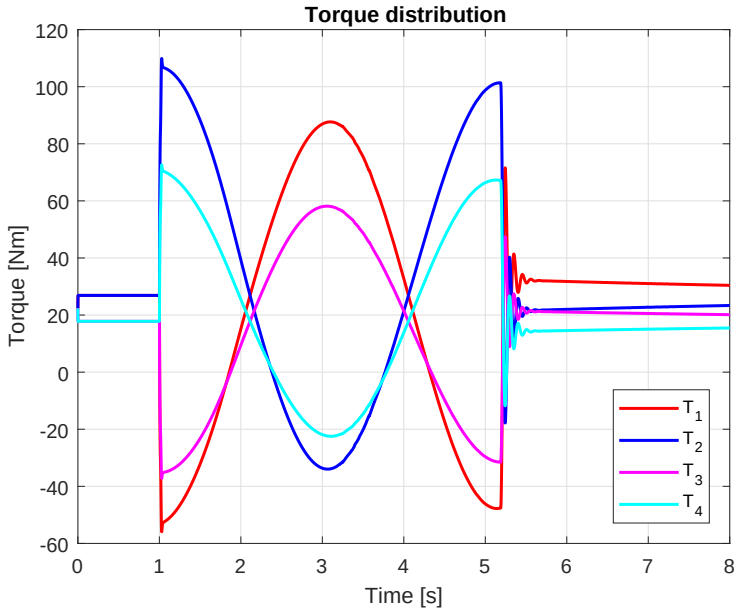

Figure 6.26: Torque allocation with ramp single lane change input, MRAC and longitudinal slip power loss based TV

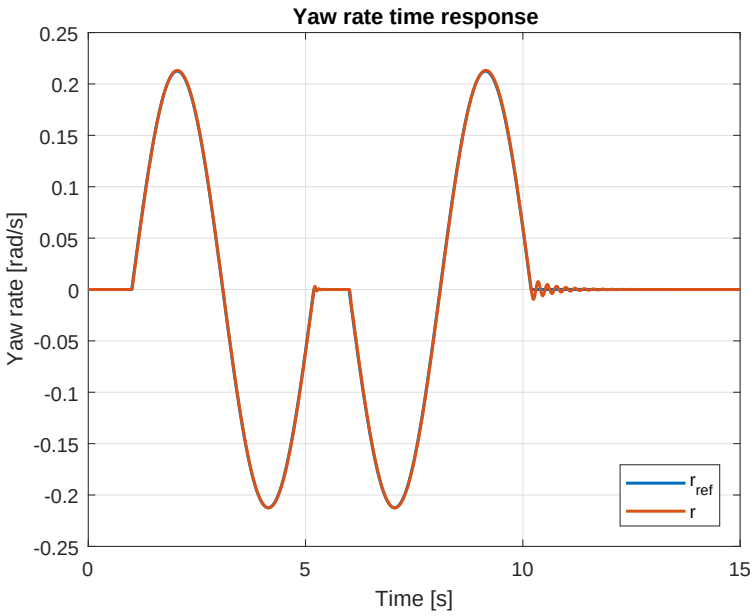

Figure 6.27: Yaw rate time response with double lane change input, MRAC and longitudinal slip power loss based TV

6.26 shows that at the end of the line change, where the curves should stabilize, they actually start oscillating with amplitudes comparable with the values reached during the maneuver in the case of the first peaks. Unfortunately a filter cannot do anything to solve the problem without worsening performances, the only solution could be the deactivation of the controller once the maneuver is over, with the intervention of a decisional algorithm as already mentioned.

The same phenomenon is even stronger in the last case, the double lane change: small chattering starts at the end of the first change and persists almost in the entire second change, before starting again at the end of it (Fig. 6.27). The same considerations could be made by looking at the torques in Fig. 6.28, the second line change should be similar to the first, with values inverted from left to right and vice versa, while the actual result presents big oscillations in the second half of the graph, and the same chattering as before when the steer angle definitively goes back to zero. None of these inconveniences could be removed with a filter without compromising tracking.

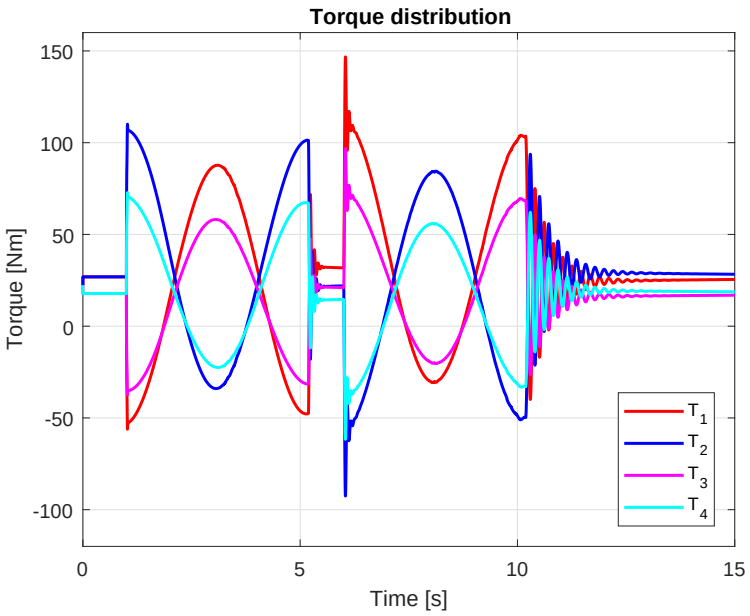

Figure 6.28: Torque allocation with ramp double lane change input, MRAC and longitudinal slip power loss based TV

6.4 Comparison with the other cost functions

All the simulations described in the previous section were repeated replacing the torque vectoring block with others implemented with the remaining cost functions. For the case of the total tire force coefficient, the general layout needed to be slightly modified: a vector containing the lateral tire forces was calculated from the vehicle plant and fed back as input for the torque allocator. During all simulations, the set of control parameters was maintained constant with respect to the analogue case with the first cost function. This was made to compare the torque curves of the three approaches in situations in which all the other conditions remained the same, so to better appreciate any differences, strengths and weaknesses. The only parameter that were modified are the cut-off frequency of the low-pass filter, according to the criterion of reducing as much as possible oscillations without compromising performances, and the tuning parameters of the three TVs. The first modification ensures that best results are being compared, while the latter is a condition that comes from the nature of the cost function, especially for the third one as explained in 6.2.3.

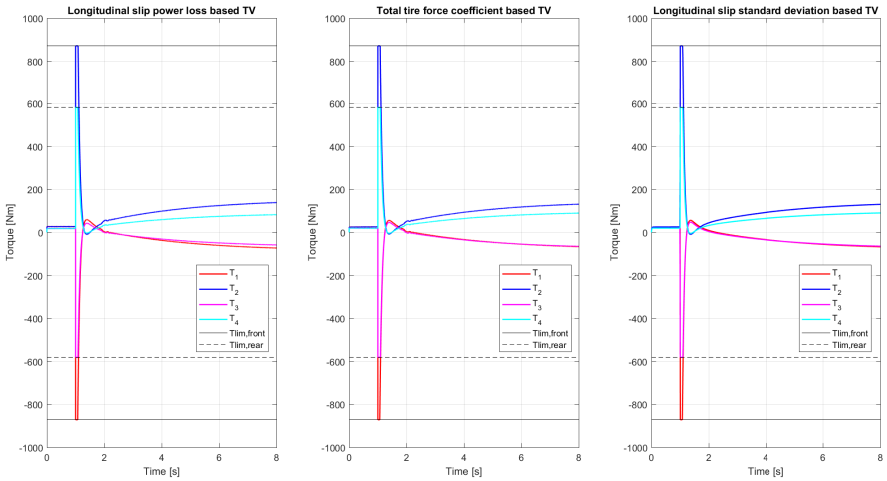

Figure 6.29: Comparison between torque allocations with the three TVs, with step input and SMC

The pattern followed in the next paragraphs is the following: for each kind of input, results of simulations with the three torque allocators will be compared, first with the use of sliding-mode control and then with MRAC. The objective is to find for every scenario the best solution or solutions among the six available. Considerations will be made about presence of harmonic features, steepness of the curves and general shape, reach of saturation and peak values, front/rear balance and physical effects on the vehicle.

As always, the first considered case is the step response. Fig. 6.29 shows the results with SMC and the three different TV strategies. First of all, the first two allocators work approximately in the same conditions with comparable results, while for the third cost function simulations could not run without setting the cut-off frequency of the filter at $1.25e^{-4}$Hz (in the first two case it was between 0.1Hz and 1Hz). This causes the SMC to start working very late, basically only the PID control is active. The consequence is that the system keeps oscillating around the final value, even though the amplitude and frequency are very small. The common feature of all graphs is the saturation in correspondence of the step, that is an expected result considering the past simulations. As regards the front/rear balance, the first cost function implies a bigger unbalance, with a 60Nm gap between the right wheels and 17Nm between the rear in the steady state zone; in the other two cases they decrease until around 40Nm and 5Nm.

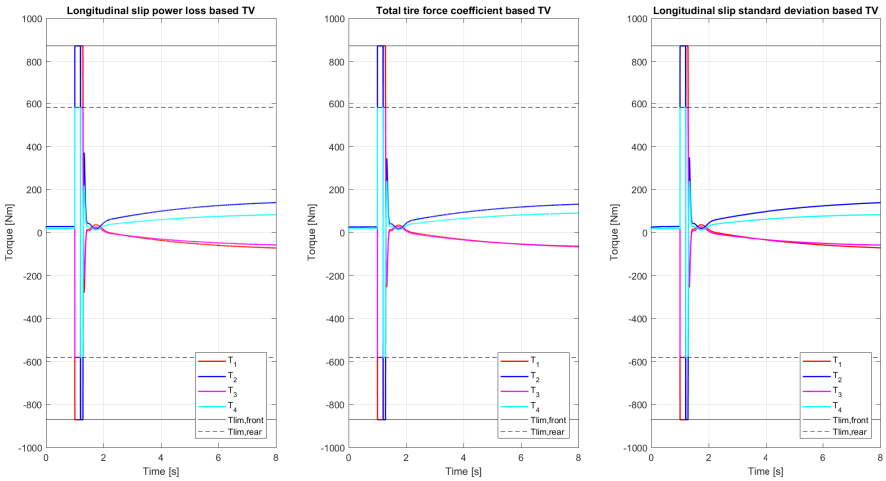

Figure 6.30: Comparison between torque allocations with the three TVs, with step input and MRAC

Fig. 6.30 instead shows the graph of the same tests but carried out with MRAC. All solutions present wide saturated zones in the first part, due to the inability of MRAC to control properly the system, while in the second part in terms of front/rear allocation the same differences as before are visible.

In this first set of assessments, sliding-mode control appeared more effective than MRAC, allocation with longitudinal slip standard deviation seemed to be much less reliable than with longitudinal slip power loss and total tire force coefficient, which showed similar performances and features.

With the J-turn simulations, more detailed information on the six proposed solutions should emerge, since the system is undergoing a maneuver that should not involve particular control problems.
The results with SMC are shown in fig 6.31: the first two solutions present very similar curves, with the same differences highlighted before, and they both present oscillations at around 2.5s. The third solution presents no chattering, but just because is weaker than the others in terms of tracking, as shown in Fig. 6.32, with the need of a strong filter that actually deactivates the sliding-mode part of the controller. Anyway, the shape of

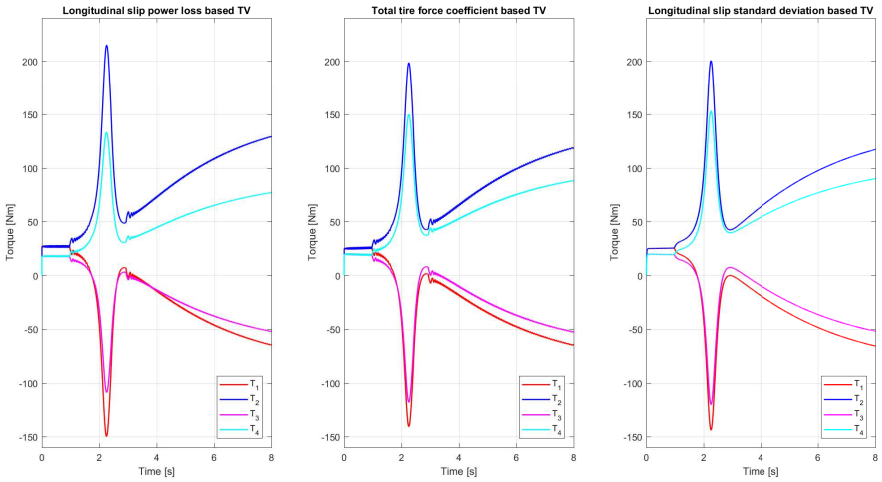

Figure 6.31: Comparison between torque allocations with the three TVs, with J-turn input and SMC

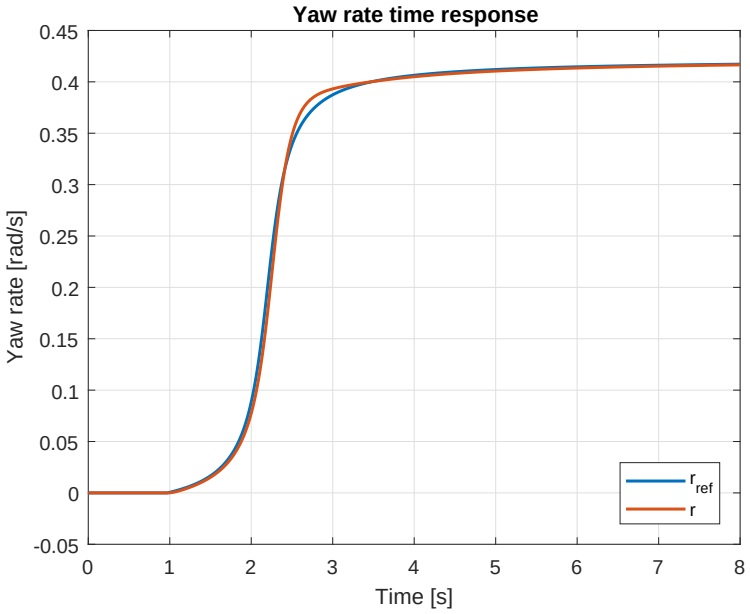

Figure 6.32: Yaw rate time response with J-turn input, SMC and longitudinal slip standard deviation based TV

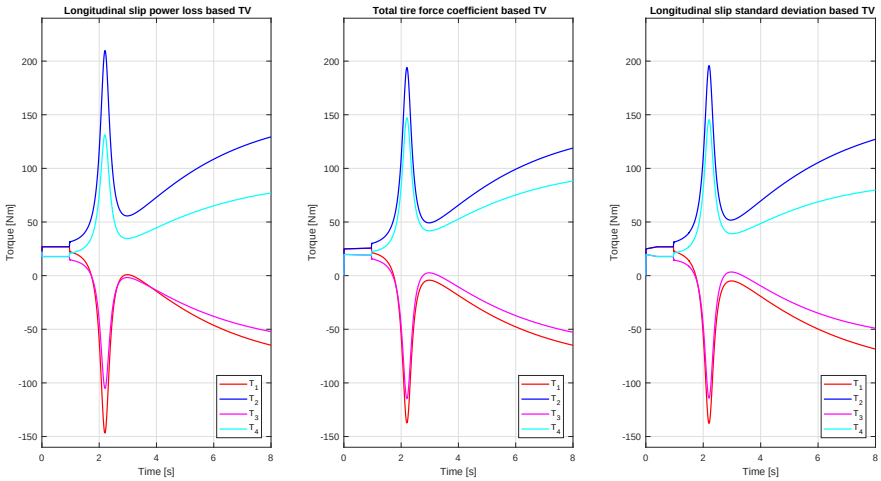

Figure 6.33: Comparison between torque allocations with the three TVs, with J-turn input and MRAC

the torque allocation is very similar to the total tire force coefficient based TV.

Shifting to the same scenario but controlled by MRAC, there are some considerable enhancements as shown in Fig. 6.33. In this specific case, MRAC ensures excellent tracking of the reference and smoothness of the torque curves. With the three objective functions, equivalent results were obtained, with only the expected difference between the first and the latter in the front/rear balancing. An interesting issue is that in the case of the second and third solutions, even though the theory behind the algorithms is totally different, during the critical part of the maneuver they lead to very similar solutions, while in the final zone the first and third graphs are closer.

Contrary to what emerged from the step response test, for J-turn MRAC is definitely preferable to SMC. This is not surprising: SMC is more powerful if the reference is steep or highly discontinuous, thanks just to its high frequency nature; on the other hand, this high frequency signal is transmitted to the state (in this case to the torque allocator) and involves problems of chattering. MRAC, instead, cannot track with high performances every kind of signal, but in many cases achieves better results without the drawback of oscillations in the control signal and in the signals downstream.

As regards the torque vectoring, the solution obtained with the total tire force co-

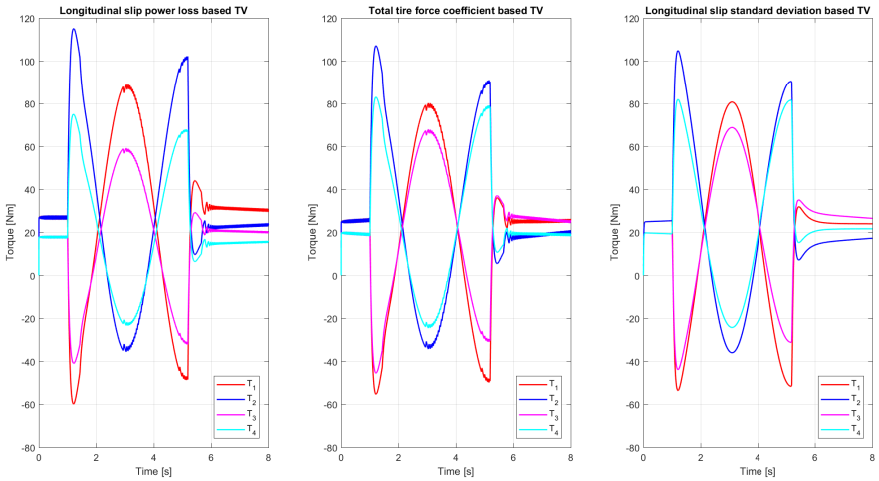

Figure 6.34: Comparison between torque allocations with the three TVs, with single lane change input and SMC

efficient is the one that requires the lowest effort by the motors and offers the most well-balanced allocation.

The last simulations deal with the single lane and double lane changes. The system controlled by SMC gave the responses in Fig. 6.34 Even though the torque curve appears better then the others, the result obtained with the longitudinal slip standard deviation cost function has to be discarded because it was impossible to achieve same tracking performances as in the other cases, as shown in Fig. 6.35.

Among the first two functions, besides the well-known differences already found and the expected chattering, it has to be noted that with the longitudinal slip power loss based allocation, at the end of the maneuver the torque values at front wheels are higher than at rear wheels, while in the other two cases the unbalance in between left and right instead of front and rear. This is probably a consequence of the oscillations in the yaw rate curve, that imply the same phenomenon in the torque vectoring input, the desired yaw moment

With MRAC, good results are achieved with all torque allocators, as it can be seen in Fig. 6.36, with just some oscillations at the end of the maneuver. The unbalances

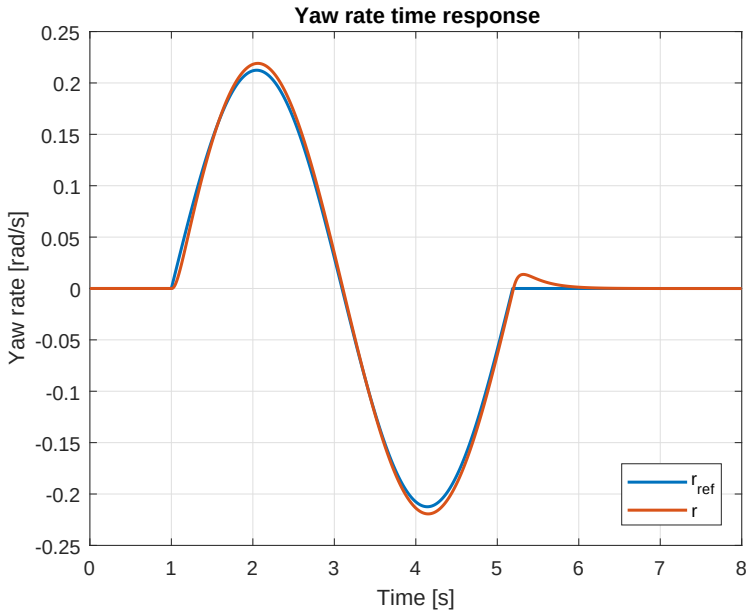

Figure 6.35: Yaw rate time response with single lane change input, SMC and longitudinal slip standard deviation based TV

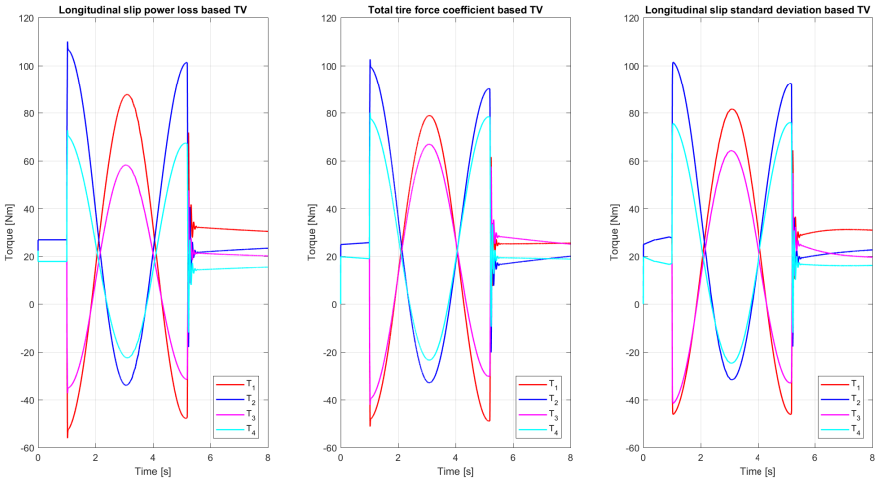

Figure 6.36: Comparison between torque allocations with the three TVs, with single lane change input and MRAC

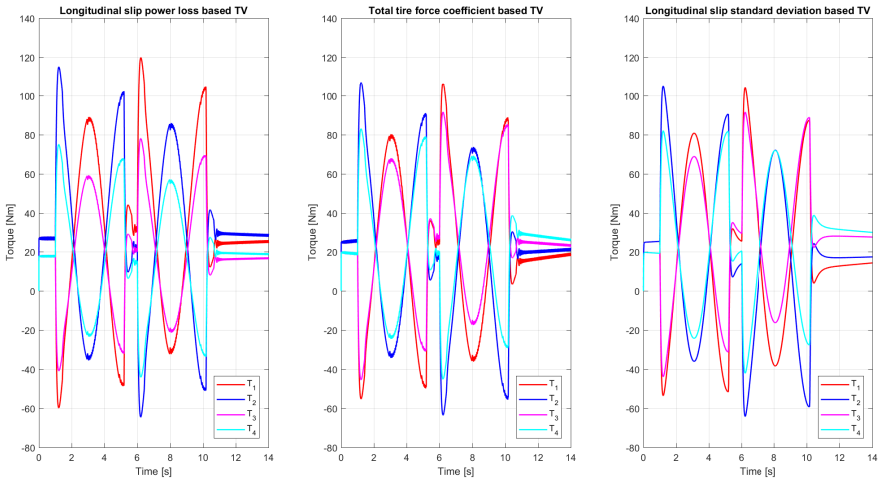

Figure 6.37: Comparison between torque allocations with the three TVs, with double lane change input and SMC

described for the SMC are present again, with the unique difference in the third graph, where the curves tend to set in the same condition as in the first case.

Facing a double lane change controlled by SMC, the system reacts as shown in Fig 6.37. Results are similar to the single lane change case: the first two functions ensure better tracking than the third; with the longitudinal slip power loss based allocation, the same torque curves are identically repeated, obviously inverted between left and right, while with the total tire force coefficient cost function the second line change provokes some slight modifications, like higher or lower peaks and different front/rear balance: for example, at the end of the maneuver with the second allocator the vehicle is now predominantly rear wheel drive.

The last case is the double lane change controlled by MRAC (Fig. 6.38). It is immediately visible that at the end of the second change, great oscillations are present in the three graphs: the reason is that the small oscillations present at the end of the single lane change persist during the entire second maneuver, even if thy are only visible in correspondence of the higher first peak; but when the yaw moment input finally drops to zero, they reappear with much grater amplitude, due to the stress undergone by the controller.

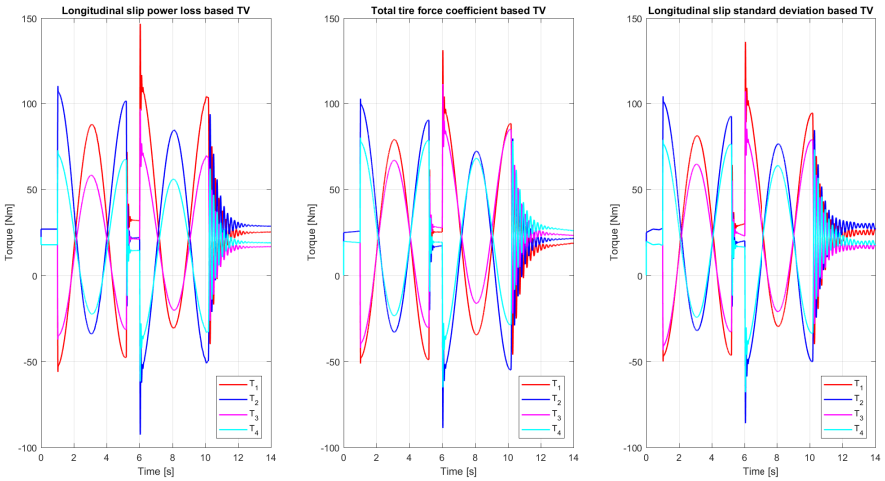

Figure 6.38: Results of simulation with step input, SMC and longitudinal slip power loss based TV

With this set of simulations it is possible to draw some conclusions on the work done. First of all, with the use of two different controllers, satisfying results were obtained in almost every case analyzed by exploiting the advantages of both of them. As already mentioned during the analysis of the results, combined PID and SMC is probably the strongest controller among the two chosen, is capable of achieving good performances also in critical situations at the expense of a system characterized by a high frequency harmonic behavior. When this situation occurred, low-pass filter were introduced to reduce oscillations as much as possible without compromising performances, with the objective of providing the motors with feasible torque curves.
MRAC, instead, involves a more complex scheme, mostly due to the presence of parameter estimators, and gives the system some different strengths and weaknesses. Generally speaking, the controller is "weaker", but in some cases achieves better results with less effort and very smooth torque curves. In addition, thanks to the parameter estimation, it is able to absorb unknown changes in the vehicle or in the environmental conditions, as long as the system does not move away too much from its initial conditions. Parameter estimation has some disadvantages too: in the last tests, it was necessary to increase a lot the values of γ_1, γ_2, γ_3 and γ_4, to obtain a faster estimation, especially using the longitudinal slip standard deviation based TV; this produces higher risks of instability

and incompatibility with the dynamics of the other components (controller, plant). For example, reducing the period if the lane changes, MRAC resulted to be incapable of controlling the system.

As regards the torque vectoring, simulations showed that gradient method used to solve the minimization problem is effective and can work in pair with the controller. Among the cost functions adopted, the second and the third gave very similar results in terms of torque curves, but the longitudinal slip standard deviation based allocation sometimes did not ensure the same performances as the others, since it ran through computational problems in presence of strong control laws. Hence, it is correct to say that the first two cost functions used are somehow better than the third. Among those, the most convenient can be chosen by looking at the real effects they would produce on a vehicle. First of all, it is necessary to say that the concept behind the obtained results is basically the same: to generate a yaw moment, the most efficient solution is to provide the outer wheels with positive torques and the inner wheels with negative torques; in this way, all wheels contribute positively to produce the desired yaw moment, so higher values in lower times can be achieved. The longitudinal slip power loss based allocation,as seen in every test, is more "aggressive", with higher torque peaks and wider gap between front and rear torques, while total tire force coefficient based allocation produces more balanced results. It has to be said that these differences affect only the motors, because the effects on the vehicle behavior are the same: in fact, the vehicle undergoes exactly the same yaw moment, that is the key variable when cornering. Hence, the final choice is between two almost equivalent solutions, with the second one slightly preferable just because it involves lower values and so lower risks of saturation and loss of performance.

Chapter 7

Budget

This project is a theoretical approach to the control of a vehicle, so it would be meaningless to develop a budget plan for its real implementation. On the contrary, an estimation of the costs involved in the realization of the thesis is presented in Table 7.1, including materials, softwares and required work time. A wage of 10€/h is supposed, considering an annual salary for a Mechanical Engineer in Spain of around 25500€[18]. The total estimated cost is of 12605,43€.

Quantity	Description	Unitary cost	Total cost
1	Medium-high performances PC	900€	900€
1	Microsoft Office 2016 - Home & Student[19]	117,71€	117,71€
1	MATLAB R2017a Education [20]	500€	500€
1	Simulink Education [20]	500€	500€
100	Initial researches and studies [h]	10€/h	1200€
400	Design and simulations [h]	10€/h	4800€
200	Thesis writing [h]	10€/h	2400€
Subtotal			9017,71€
VAT 21%			1893,72€
Total			12605,43€

Table 7.1: Cost estimation

Chapter 8

Conclusions and future developments

8.1 Conclusions

The objective of this work was to design the control of a 4MIDEV including two main components: the controller itself and an optimal torque allocator, to exploit as much as possible the advantages of equipping the vehicle with independent electric motors. The key issue of the project was to combine the two components with a real-time cooperation: the controller feeds the torque allocator with a continuous signal and the torque allocator provides the motors the optimal torque repartition to follow the control law. To make this possible, the TV dynamics need to be much faster than the controlled system dynamics. Concretely, this coincided with the design of a method to solve fast an optimization problem. Gradient method was selected as solution, with three different cost functions on which the optimization problem could have been based. After the simulations described in section 6.2 it was possible to certify that gradient method is a valid solution: it permits to find the optimal solution and the designed tuner aimed at reducing computational times proved to be efficient and extremely useful. Hence, it was finally possible to connect the plant, the torque allocator and the proposed controllers to develop the design of these latter and finally test them.

Satisfying results were achieved both in terms of control and torque vectoring, in any of the considered cases there was at least one acceptable solution. Two of the allocators implemented proved to be more reliable and efficient than the other, and matched with

similar performances with the controllers. Due to the restricted set of simulations (compared with the number of possible real maneuvers), it is not possible to find a definitive unique solution with high performances and reliability. The contribution of this work is thus the prove that the proposed solutions to control a 4MIDEV with an optimal torque distribution are actually valuable and feasible under the taken hypotheses. The system worked with a non-linear vehicle plant, that included the Pacejka's tire model and the contributions of the steer angle seen as a disturbance and not as a control variable.

The biggest limitation to this project is the absence of a real system (vehicle and environment), or at least a specific vehicles simulator. Furthermore, some restrictive hypotheses were taken, like constant speed and negligible vertical dynamics. Undoubtedly, with a real model or a high precision simulator, all vehicle features could be included to obtain a more reliable and realistic scenario, comprehensive of any dynamics and interactions between components. As regards the controllers, it has to be said that every test needed a specific tuning process to reach the optimal solution; hence, there is not a unique set of parameters that ensures good tracking in any situation, even though it is possible to find a solution which implies acceptable (non optimal) performances with any scenario.

8.2 Future developments

In order to make the system more realistic, the first step would be to substitute the vehicle model with a specific car simulator (as could be CarSim or CarMaker softwares). With this improvement, all vehicle dynamics would be included and considered, thus obtaining more reliable and realistic simulations. Same considerations can be made for the input curves of the tests: amplifying the range of maneuvers, richer information about the actual capabilities of the controllers could be collected, and it could be easier, if possible, to obtain a universal set of control parameters suitable for any conditions.

Another interesting issue is the study of the behavior of the system with changing environmental conditions. For example, all tests could be repeated with different road parameters, simulating slippery asphalt or different road surfaces. With this procedure, the limit conditions for the controllability of the system could be discovered, and then

tests with changing parameters during the simulations could be implemented. For example, scenarios like a sudden change of surface, a pool of water or an unexpected loss of adherence of a single tire could be reproduced. A good controller should be capable of reacting against this kind of situations with robust and efficient performances; especially MRAC should be particularly indicated thanks to the parameter estimation.

Looking at the results of the simulations in Chapter 6, there are some cases of undesired oscillations at the end of the maneuver (especially with lane changes). Beyond the already mentioned introduction of a decisional algorithm to activate/deactivate the controller [8], perhaps a system capable of detecting and eliminating those oscillations could be designed.

In conclusion, this project laid the foundations for a much wider study. All the modifications and enhancements with the objective of expand the range of validity of the work should be implemented. Starting with the extension of simulated scenarios and the elimination of some restrictive hypotheses, the model could be then tested on a high performance simulator and gradually modified to make it more and more realistic, perhaps with the final objective of implementation and experimental validation on a real vehicle.

Acknowledgments

I would like to express sincere thanks to my supervisor Eng. Davide Tarsitano from my home university Politecnico di Milano.

Bibliography

[1] Andy Watts, Andrew Vallance, Andrew Whitehead, Chris Hilton and Al Fraser, "The Technology and Economics of In-Wheel Motors", SAE International, October 2010.

[2] Richard Hurdwell, Martyn Anderson, "Dynamics of Vehicles With In-wheel Motors", lecture at Cambridge University, April 2011.

[3] Dr. C. Hilton, "Wheel Torque and Speed in a Vehicle with In-Wheel Motors", Protean Electric Ltd, May 2016, www.proteanelectric.com.

[4] Elaphe Ltd. Website, http://in-wheel.com/product-category/motors/.

[5] Leonardo De Novellis, Member IEEE, Aldo Sorniotti, Member, IEEE, and Patrick Gruber, "Wheel Torque Distribution Criteria for Electric Vehicles With Torque-Vectoring Differentials", IEEE Transactions on Vehicular Technology, Vol. 63, No. 4, pp. 1593-1602, May 2014.

[6] Cheng Lin and Zhifeng Xu, "Wheel Torque Distribution of Four-Wheel-Drive Electric Vehicles Based on Multi-Objective Optimization", Energies 2015, vol. 8, pp. 3815-3831, April 2015.

[7] Leonardo De Novellis, Aldo Sorniotti, Patrick Gruber, Javier Orus, Jose-Manuel Rodriguez Fortun, Johan Theunissen, Jasper De Smet, "Direct yaw moment control actuated through electric drivetrains and friction brakes: Theoretical design and experimental assessment", ScienceDirect Mechatronics Journal, Vol. 26, pp. 1-15, March 2015.

[8] Li Zhai, Member IEEE, Tianmin Sun and Jie Wang, "Electronic Stability Control Based on Motor Driving and Braking Torque Distribution for a Four In-Wheel Motor

Drive Electric Vehicle", IEEE Transactions on Vehicular Technology, Vol. 65, No. 6, pp. 4726-4739, June 2016.

[9] Tommaso Goggia, Aldo Sorniotti, Member IEEE, Leonardo De Novellis, Member IEEE, Antonella Ferrara, Senior Member IEEE, Patrick Gruber, Johan Theunissen, Dirk Steenbeke, Bernhard Knauder, and Josef Zehetner, Member IEEE, "Integral Sliding Mode for the Torque-Vectoring Control of Fully Electric Vehicles: Theoretical Design and Experimental Assessment", IEEE Transactions on Vehicular Technology, Vol. 64, No. 5, pp. 1701-1715, May 2015.

[10] Dong-Hyung Kim, Chang-Jun Kim, Sang-Ho Kim, Joo-Young Choi, and Chang-Soo Han, Member IEEE, "Development of Adaptive Direct Yaw-moment Control Method for Electric Vehicle based on Identification of Yaw-rate Model", 2011 IEEE Intelligent Vehicles Symposium (IV) Baden-Baden, Germany, pp. 1098-1103, June 2011.

[11] Rajesh Rajamani, "Vehicle Dynamics and Control", Chapters 3, 4, 8, 13, 2006.

[12] Thanh Vo-Duy and Minh C. Ta, "A Universal Dynamic and Kinematic Model of Vehicles", IEEE Vehicle Power and Propulsion Conference (VPPC), December 2015.

[13] H. Pacejka, E. Bakker, L. Nyborg, "Tire modeling for use in vehicle dynamics studies", SAE Paper No. 870421, 1987.

[14] A. Cherukuri, E. Mallada, and J. Cortes, "Asymptotic convergence of constrained primal-dual dynamics", Systems & Control Letters, Vol. 87, pp. 10-15, 2016.

[15] D. Feijer and F. Paganini, "Stability of primal-dual gradient dynamics and applications to network optimization", Automatica, Vol. 46, pp. 1974?1981, 2010.

[16] Petros Ioannou, "The Control Handbook", Chapter 54, 1996.

[17] Kiumars Jalali, Thomas Uchida, John McPhee, Steve Lambert, "Development of an Advanced Fuzzy Active Steering Controller and a Novel Method to Tune the Fuzzy Controller", SAE International, April 2013.

[18] www.payscale.com

[19] https://products.office.com/es/home-and-student

[20] https://es.mathworks.com/academia/student_version.html